


# A Framework for Simulating the Evolution of Underwater Landslides and Its Application to Slope Failures in Swiss Lakes

**Journal Article****Author(s):**

Stoecklin, Andreas; [Puzrin, Alexander](#) 

**Publication date:**

2023-12

**Permanent link:**

<https://doi.org/10.3929/ethz-b-000638274>

**Rights / license:**

[Creative Commons Attribution 4.0 International](#)

**Originally published in:**

Journal of Geotechnical and Geoenvironmental Engineering 149(12), <https://doi.org/10.1061/JGGEFK.GTENG-11497>

**Funding acknowledgement:**

168998 - Dynamic evolution of submarine landslides (SNF)



# A Framework for Simulating the Evolution of Underwater Landslides and Its Application to Slope Failures in Swiss Lakes

Andreas Stoecklin, Ph.D.<sup>1</sup>; and Alexander M. Puzrin, Ph.D.<sup>2</sup>

**Abstract:** Destructive underwater mass movements can impose a threat to off-shore infrastructure and near-shore communities. Yet predicting their formation and failure mechanisms remains a major challenge, in part due of the large variety of factors affecting their stability over time. Long-term processes such as sedimentation as well as short-term events such as earthquakes can impact the stability of the slope highlighting the need for an integrated analysis procedure to quantify their impact. In this article, such a framework is presented to simulate the evolution of subaqueous landslides, ranging from sediment deposition to seismic triggering to the postfailure evolution of the collapsing soil mass. Each stage is simulated in an individual step, based on different finite element-based methodologies, to best model the governing processes. The steps are linked in a consistent manner to facilitate the simulation of the landslide evolution as a continuous process. The presented framework is applied to analyze three historical landslide events in Swiss lakes. The model predictions compare well with the in situ landslide deposits. The simulation results provide insight into slope failure mechanisms and effects of seismic ground motion characteristics on the stability of the analyzed slope failures. DOI: [10.1061/JGGEFK.GTENG-11497](https://doi.org/10.1061/JGGEFK.GTENG-11497). © 2023 American Society of Civil Engineers.

**Author keywords:** Landslides; Failure; Slopes; Numerical modeling; Finite-element modeling; Offshore engineering.

## Introduction

One of the major natural hazards in the offshore environment is imposed by destructive underwater landslides. They are known to damage off-shore infrastructure such as platforms, underwater cables, and pipelines (Carter et al. 2012; Fine et al. 2005; Fryer et al. 2004; Tappin et al. 2001). The damage to pipelines caused by submarine mass movements alone was estimated at about \$400 million annually (Mosher et al. 2010). Furthermore, underwater landslides can act as a source of destructive tsunamis in the sea (Fine et al. 2005; Fryer et al. 2004; Tappin et al. 2001) and, on a smaller scale, in Alpine lakes (Schnellmann et al. 2002; Strasser et al. 2007). With the growing importance of offshore infrastructure and costal developments, the potential for damage caused by submarine landslide events is likely to increase in the future. This highlights the need to better understand the processes controlling their behavior and to develop suitable tools for reliable hazard assessments and for the design of effective mitigation measures.

## Evolution of Underwater Landslides

Numerous research efforts have been devoted to investigate the causes of submarine mass movements (Hampton et al. 1996;

Locat and Lee 2002). Earthquake events are recognized as one of the most common triggers of underwater landslides, influencing the short-term slope stability due to the ground motion as well as the long-term stability due to the gradual buildup of excess pore pressures (Masson et al. 2006). Yet, seismic loading is only one factor in a chain of processes involved in submarine landsliding and, on its own, often fails to explain observed landslide phenomena. Some slopes, for instance, show traces of repetitive landsliding, whereas neighboring slopes, exposed to similar seismicity, have remained stable over thousands of years (Fisher et al. 2005; Masson et al. 2002). Furthermore, observations have revealed that the recurrence intervals of repetitive landslides often do not match the return period of the triggering event (Fisher et al. 2005; Strasser et al. 2012; Völker et al. 2011). These observations can be better explained by preconditioning processes, which can condition sediments over extended time periods and create an environment for slope failures, until a short-term event, such as an earthquake, eventually initiates the mass movement. In many cases it is, in fact, believed that preconditioning plays a dominating role, and the actual triggering mechanism can be of subordinate importance (Mosher et al. 2010). There are many known preconditioning factors, such as rapid sedimentation, gas hydrate dissociation, groundwater flow, and seismic activity (Lee et al. 2007). Their common feature is a gradual buildup of excess pore water pressures, reducing the effective stress and hence the shear resistance of the sediments. Amongst them, rapid sedimentation is one of the most common preconditioning factors. If sediments are deposited on slopes at a fast rate, there may not be sufficient time for the pore fluid within the underlying sediments to drain toward the seafloor. This can lead to a gradual buildup of excess pore pressures and a relative weakening of the slope (e.g., Dugan and Sheahan 2012).

Underwater mass movements are therefore often regarded as evolving processes, ranging from deposition and preconditioning of sediments to fracturing of an initial failure zone to failure propagation and postfailure evolution into different patterns (Locat and Lee 2002; Vanneste et al. 2014). A schematic illustration of a

<sup>1</sup>Scientific Assistant, Institute for Geotechnical Engineering, Eidgenössische Technische Hochschule (ETH) Zurich, Zurich CH-8093, Switzerland (corresponding author). ORCID: <https://orcid.org/0000-0002-2095-056X>. Email: [andreas.stoecklin@igt.baug.ethz.ch](mailto:andreas.stoecklin@igt.baug.ethz.ch)

<sup>2</sup>Professor, Institute for Geotechnical Engineering, Eidgenössische Technische Hochschule (ETH) Zurich, Zurich CH-8093, Switzerland. ORCID: <https://orcid.org/0000-0002-9566-8841>. Email: [alexander.puzrin@igt.baug.ethz.ch](mailto:alexander.puzrin@igt.baug.ethz.ch)

Note. This manuscript was submitted on November 18, 2022; approved on July 19, 2023; published online on October 5, 2023. Discussion period open until March 5, 2024; separate discussions must be submitted for individual papers. This paper is part of the *Journal of Geotechnical and Geoenvironmental Engineering*, © ASCE, ISSN 1090-0241.

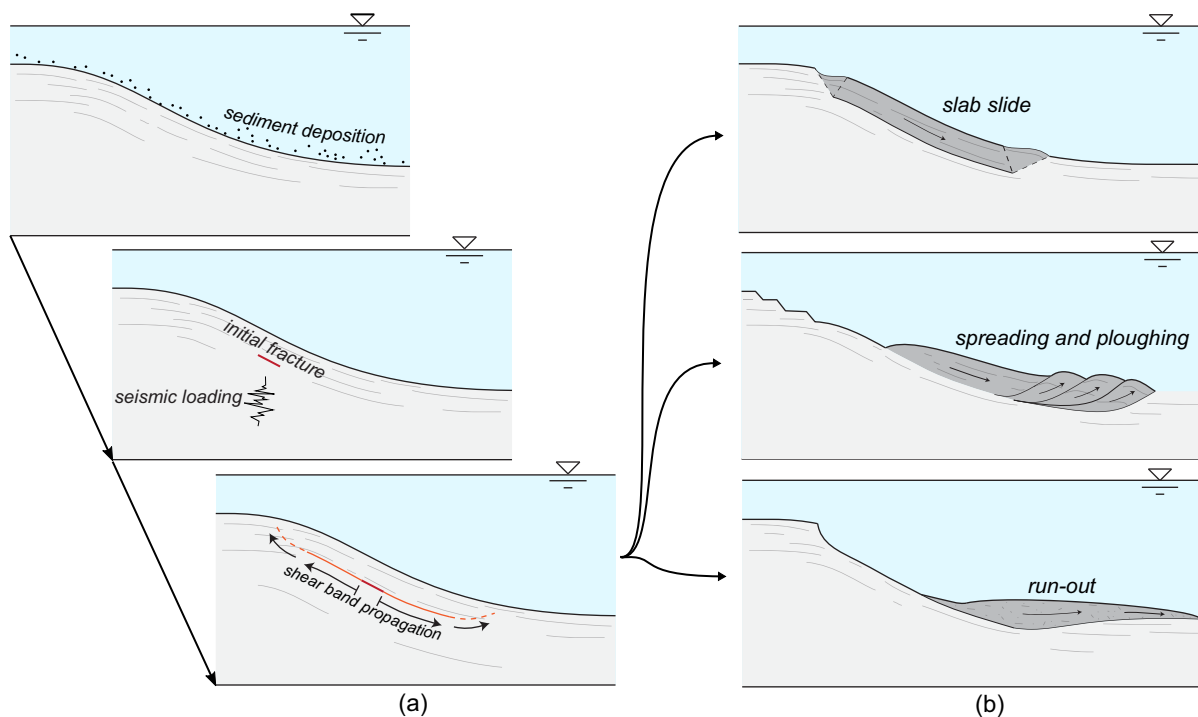


**Fig. 1.** Illustration of different stages of submarine landslide evolution patterns described by Puzrin et al. (2016): (a) sediment deposition and failure initiation and propagation; and (b) global failure and evolution into different postfailure patterns.

possible landslide evolution is depicted in Fig. 1. For reliable assessments of the hazards imposed by submerged slopes, the relevant processes in the landslide evolution therefore must be understood and accounted for.

### Advances in Mechanical Modeling

Mechanical models provide an essential tool for analyzing the behavior of historic slides and, to some extent, predicting the behavior of potential future events. Numerous models and methodologies have been developed in recent years to describe and simulate different processes involved in subaqueous mass wasting. A number of key studies are listed below, categorized according to the evolution stages illustrated in Fig. 1.

- Preconditioning by rapid sedimentation: Motivated by problems encountered by drilling in overpressured sediments, increasingly sophisticated mechanical models have been developed to simulate the development of excess pore pressures in soil layers due to fast deposition of new sediments on the sea floor (Audet and Fowler 1992; Gibson 1958; Wangen 1992). Similar models were later applied to investigate the effect of sedimentation-induced overpressures on the stability of submerged slopes in several studies (e.g., Stigall and Dugan 2010; Viesca and Rice 2012).
- Failure initiation and seismic triggering: The dynamic response of submarine slope profiles has been analyzed in multiple studies to investigate the seismic triggering process (Biscontin et al. 2004; Biscontin and Pestana 2006; Nadim et al. 2007; Puzrin et al. 1997; Zhou et al. 2017). The results presented in these studies highlight important aspects that govern the seismic response of submerged slopes, such as the effect of cyclic generation of excess pore pressures, the influence of ground motion characteristics, or the effect of preexisting weak layers.
- Propagation of failure zones: Once a failure zone is initiated, it can evolve progressively through the process of shear band

propagation (Palmer and Rice 1973). For sediments that exhibit strain softening behavior, it has been demonstrated that, once the shear band exceeds a certain critical length, the propagation progresses under constant external forces, resulting in a self-driven, catastrophic failure of the slope (Germanovich et al. 2016; Puzrin et al. 2004; Viesca and Rice 2012; Zhang et al. 2015). If a weak layer exists within the soil deposit, shear band can propagate into stable parts of the slope, thus predicting larger landslide bodies and providing a possible mechanism to explain the enormous sizes of some observed landslide scars (Puzrin et al. 2015, 2016; Zhang et al. 2017).

- Global failure and postfailure evolution: Once the shear band reaches the seafloor, a failure mechanism is formed, marking the point of global failure (Puzrin et al. 2016). The landslide can evolve into different patterns, such as ploughing and retrogressive failures, runouts and turbidity currents, or a combination of different types (see Fig. 1). Different mechanical models have been developed, which help in explaining these phenomena and identifying controls for different postfailure evolution patterns (e.g., Buss et al. 2019; Dey et al. 2015; Kvalstad et al. 2005; Puzrin et al. 2016; Zhang et al. 2019). To analyze the postfailure motion of mass movements, different numerical modeling approaches exist (Soga et al. 2016). Amongst them, models based on the material point method have been developed recently to simulate the seismic triggering and subsequent large-deformation runout of onshore landslides within a single analysis step (Alsardi et al. 2021; Kohler et al. 2022).

These models provide essential tools for understanding the mechanisms involved in underwater slope failures and quantifying their effect. Yet, they are focused on modelling particular stages of the landslide evolution. To simulate the process as a whole and quantify the relative effects of different mechanisms involved in the formation of underwater mass movements, a combined analysis approach is required.

## Goals and Motivation

In this study, such a combined analysis procedure is presented. The landslide evolution is simulated in a sequence of analysis steps, ranging from sediment deposition to seismic triggering to postfailure evolution. Different finite element (FE)-based methodologies are employed to best model for the governing processes at any stage of the evolution. The individual steps are linked together, forming a consistent framework to analyze the landslide evolution as a continuous process. The framework thus facilitates the quantification of effects of sedimentation and seismic loading on the postfailure kinematics of underwater mass movements. The framework is applied to analyze three historical underwater landslide events in Swiss lakes. To assess the accuracy of the model results, the predicted postfailure landslide geometries are compared with the actual in situ landslide deposits of the analyzed cases.

## Description of the Analyzed Cases

Three historical underwater landslides were analyzed in this study, i.e., the two Zinnen slides in Lake Lucerne and the Oberrieden 2 Slide in Lake Zurich. These historical landslides present suitable case studies, since (1) the slides were triggered by earthquakes, (2) the sites have been investigated in the past, providing the required information to determine the simulation input parameters, and (3) the slides are relatively uniform in the lateral extent, thus justifying a plane-strain analysis.

### Zinnen Slides

The Zinnen slides are located in Lake Lucerne within the Küssnacht Basin. The ground consists of a molassic bedrock, which is covered by fine-grained glacial-to-postglacial sediments, consisting of silty clays and clayey silts with a thickness of <8 m on the lateral slopes (Sammartini et al. 2021; Strasser et al. 2007, 2011). The basal shear surface evolved near the bottom of the sediment layer between the late glacial and the postglacial units (Sammartini et al. 2021). In this study, the Zinnen Main and the Zinnen Baby Slide are analyzed [see Fig. 2(a)]. The slopes of both slides are steep, inclined by up to 32° and 36° [see Figs. 2(c and d)]. The thickness of the sliding layer was estimated at ~6 m for the main and ~5 m for the Baby Slide (Sammartini et al. 2021). The Zinnen slides were most likely triggered by an earthquake event in 1,601 with a moment magnitude of  $M = 5.9$ , which led to the collapse of several slopes in Lake Lucerne (Kremer et al. 2017; Schnellmann et al. 2006). A more detailed description of the slides was provided by Sammartini et al. (2021). The two slides show distinctly different runout lengths despite the close proximity and similar slope gradients. They thus offer a suitable case study to test whether the procedure allows predicting these differences with the same set of parameters. To build the computational models, the prefailure lake bottom geometry was reconstructed by connecting the intact regions on adjacent parts of the slope, as shown in Fig. 2(b). The same procedure was applied in a separate study, where the frontal emplacement style of the Zinnen Main Slide was investigated (Klein et al. 2022). The resulting cross sections, which provided the basis for the computational models, are shown in Figs. 2(c and d). A preexisting inherit weaker layer was included near the base of the sediment layer, to account for the lower shear resistance in the lower late glacial unit compared with the overlying Holocene unit (Sammartini et al. 2021).

### Oberrieden Slides

The two Oberrieden slides are located on the southwestern flank of Lake Zurich offshore the village of Oberrieden. The Oberrieden Slide 1 occurred in 1918 A.D. and was triggered by human activity, whereas the Oberrieden Slide 2 is believed to have been triggered by an earthquake about 2210 yr. B.P. (Strasser and Anselmetti 2008; Strupler et al. 2017). Since this study is focused on earthquake-triggered slides, only the Oberrieden Slide 2 was analyzed. The failure scar extends laterally ~400 m and the distance from head scarp to toe measures ~770 m (see Fig. 3). The soil profile consists of glacial and postglacial sediments with a thickness of about 5–7 m (measured in the undisturbed sediments adjacent to the slide) overlying the molassic bedrock (Strupler et al. 2017). The slope gradient is much milder than for the Zinnen slides, measuring about 12° for the upper and lower parts of the slope, and the middle part is inclined by about 6°. The reconstructed prefailure slope geometry was obtained by connecting the level contour lines of the adjacent intact parts of the slope [see Fig. 3(b)]. A more detailed description of the slides was provided by Strupler et al. (2017). The cross section, from which the 2D computational model was built, is shown in Fig. 3(c). Similar to the Zinnen slides, an inherit weak layer was included near the base of the sediment layer (see Fig. 12 in Appendix II).

## Description of the Three-Step Methodology

The landslide evolution is simulated in a sequence of three main steps:

1. Sedimentation analysis: The sediment buildup on the slope over time is simulated [see Fig. 4(a)].
2. Seismic analysis: The earthquake-induced initiation and triggering of the slide are simulated [see Fig. 4(b)].
3. Postfailure analysis: The Self-driven motion of the collapsing slope is simulated until its arrest [see Fig. 4(c)].

In each step, different processes play a governing role, requiring different methodologies to model the problem as accurately as possible. The individual steps are computed using the ABAQUS computing software (Dassault Systèmes 2014) and connected by prescribing the final result of the preceding step as initial conditions to the subsequent step in a consistent manner. The basic principle of the proposed three-step procedure has initially been outlined in a conference paper by Stoecklin and Puzrin (2020) and is subsequently described in more detail. A simplified version of the procedure, where the sedimentation analysis was replaced with a basic static Lagrangian analysis step, has been compared and validated against simulations carried out with an independent approach based on the material point method (Kohler et al. 2022). The solutions obtained with the two independent approaches compare well for the co- and postseismic analysis in terms of the time of triggering, the resulting failure mechanism, and the resulting postfailure geometry. In the following, the applied FE methodologies for the three steps are briefly described.

### Step 1: Sedimentation Analysis

In this first step, the deposition of sediments on the slope over time and buildup of a sediment layer is modeled. This constitutes a non-linear consolidation problem with a moving boundary, which is solved using a coupled hydromechanical, updated Lagrangian, static, implicit finite element approach. Elements are activated and stacked on top of older elements in a sequence of steps to simulate the continuous sediment buildup process, while maintaining a zero excess pore water pressure hydraulic boundary condition at the



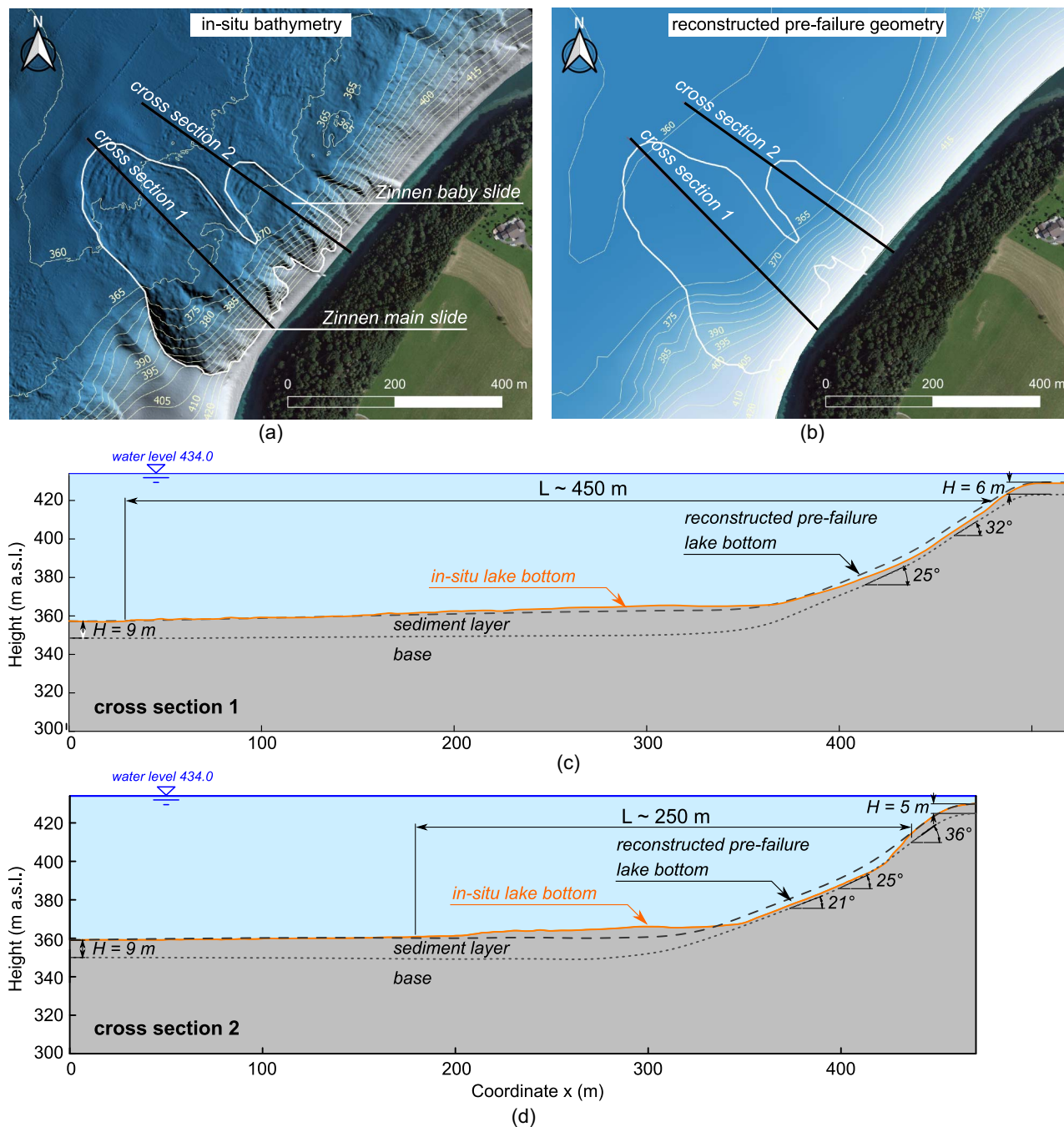


**Fig. 2.** Illustration of the Zinnen slides: (a) in situ slope geometry; (b) reconstructed prefailure slope geometry; (c) cross-section through the Zinnen Main Slide; and (d) the Zinnen Baby Slide. (Map © Federal Office of Topography swisstopo 2019, © Data swisstopo, FOT.)

moving seafloor [see Fig. 5(a)]. The procedure is described in more detail by Stoecklin et al. (2017). As fresh sediments are deposited on the lake or seafloor, the underlying soil is loaded and compressed as the pore fluid drains toward the seafloor. If the rate of sediment deposition is fast, compared with the hydraulic conductivity of the sediments, this can lead to the buildup of excess pore water pressure within the slope and an increased susceptibility to slope failure. For low deposition rates, the process results in a fully consolidated soil deposit. The sedimentation analysis facilitates computing the evolution of the effective stress field within the slope as the sediment layer grows in thickness over time along with a gradual buildup of overpressures. It therefore provides the modeled

prefailure in situ conditions [see Fig. 5(b)]. These results are then processed and prescribed as initial conditions for the subsequent analysis step.

Note that, for the cases analyzed in this study, the sedimentation-induced overpressures on the slope are negligible due to the low sediment deposition rate. Hence, the stress-conditions are almost fully drained prior to the seismic loading. The sedimentation simulation could, therefore, also have been performed with a simpler single-phase mechanical FE approach. Nonetheless, for other cases overpressures from rapid sedimentation can be significant, requiring the coupled simulation procedure described above to account for this effect.

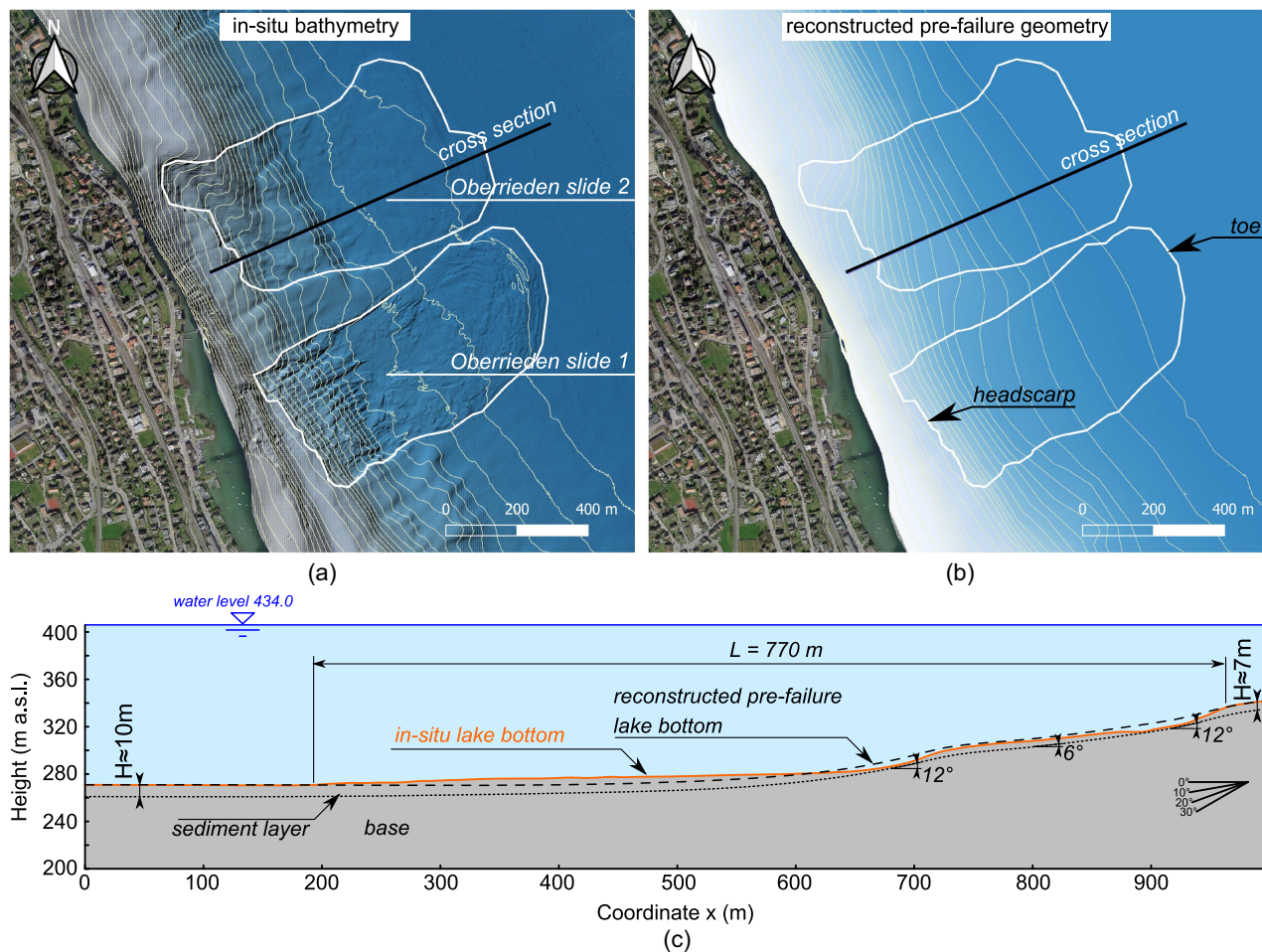


**Fig. 3.** Illustration of the Oberrieden slides: (a) in situ slope geometry; (b) reconstructed prefailure slope geometry; and (c) cross section on which the simulation is based. (Map © Federal Office of Topography swisstopo 2019, © Data swisstopo, FOT.)

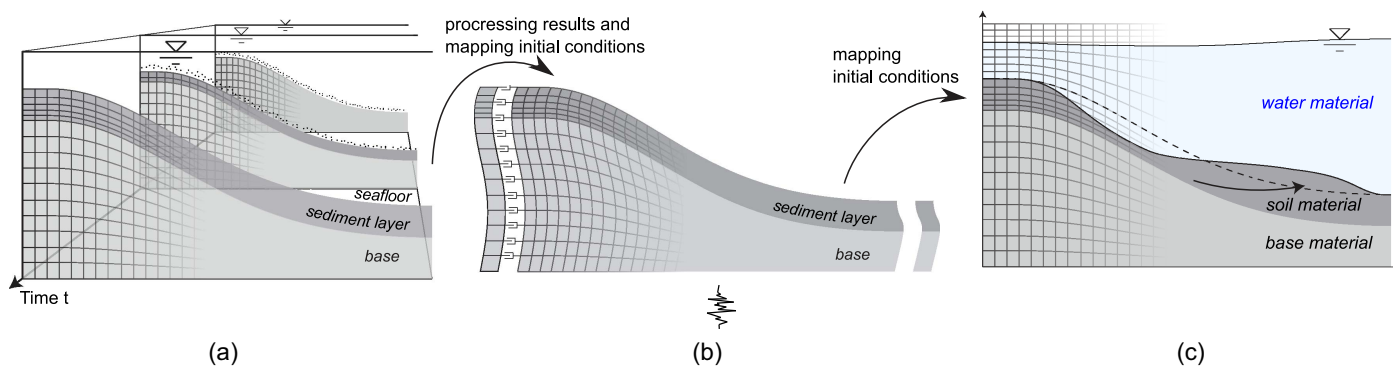


**Fig. 4.** Illustration of the three-step analysis procedure: (a) sedimentation analysis to compute prefailure slope conditions; (b) seismic analysis to model the triggering and initiation of the slope failure; and (c) postfailure analysis to simulate the evolution of the collapsing soil mass.

### Step 2: Seismic Analysis

With the seismic analysis, the impact of an earthquake event on the slope is analyzed at a specific stage in the sediment buildup process. The seismic excitation leads to fast, essentially undrained loading of the saturated sediments, which is why this process is simulated using a dynamic, implicit total stress-based FE analysis approach. With this approach, excess pore water pressures developing during seismic loading are treated as an internal variable at

each integration point and fluid-flow along with a redistribution of excess pore water pressures are neglected during seismic excitation.

**Initial and loading conditions:** The initial, static total stress tensor  $\sigma_0^{\text{tot}}$  for the seismic analysis was derived from the sedimentation analysis results at each integration point as the sum of the initial effective stress tensor  $\sigma_0$ , the hydrostatic water pressure  $u_{\text{hyd}}$ , and the initial excess pore water pressure  $\Delta u_0$  from the sedimentation process as

$$\sigma_0^{\text{tot}} = \sigma_0 + (u_{\text{hyd}} + \Delta u_0)\mathbf{1} \quad (1)$$

where  $\mathbf{1}$  = the second-order identity tensor. Similarly, the density of the sediments at each integration point in the model was derived from the void ratio that results from the sedimentation analysis as

$$\rho = \frac{G_s + e}{1 + e} \rho_w \quad (2)$$

where  $\rho_w$  = fluid density;  $G_s$  = specific gravity of grains; and  $e$  = void ratio at the end of the sedimentation analysis. The density and initial static stress field were prescribed to the model as initial conditions, and gravitational loading was applied to the model as an instantaneous, uniform, vertical acceleration. To equilibrate the static stress field, nodal forces are applied at the model boundaries. These nodal forces correspond to the sum of the boundary reaction forces from the sedimentation analysis and the hydrostatic water pressure (see Fig. 6). The forces were kept constant throughout the seismic analysis. This procedure is not entirely accurate for the material in the sediment layer, which can experience yielding and hence a change in the lateral stress. Nevertheless, the implication on the overall behavior of the main slope is considered small,

provided that the lateral boundaries are placed far enough away from the main region of interest. The water was represented only as a hydrostatic pressure, thus neglecting inertia effects and viscous drag forces of the water at the lake bottom. Since the seismic slope deformation occur predominantly in a slope-parallel direction and the viscous drag forces are considered small compared with the shear resistance of the soil, this simplification is considered justified for the seismic analysis (in contrast with the postfailure analysis).

**Boundary conditions:** At the lateral boundaries of the model, the free-field boundary method was applied to avoid the reflection of outgoing stress-waves without restricting the free-field movement of the ground (Zienkiewicz et al. 1989). The free-field columns at each side of the main model consist of a single column of stacked elements. Their rotational degrees of freedom are constrained, and the translational degrees of freedom of the nodes on one side are tied to the corresponding nodes on the opposite side of the column. To ensure that the motion of the free-field columns is not significantly affected by the deformation of the main model but not the other way around, a large out-of-plane thickness is assigned to the free-field columns. Free-field columns are connected to the main model at the lateral boundaries with dashpot elements (see Fig. 6)

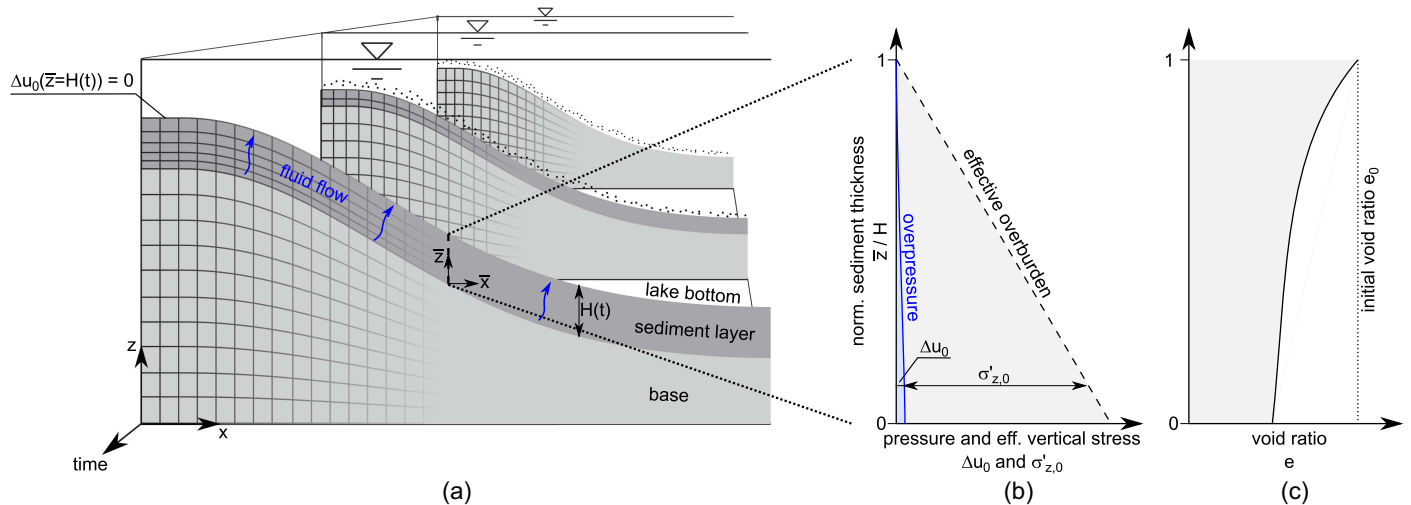


**Fig. 5.** Illustration of (a) the sedimentation FE model; (b) the resulting stress field; and (c) void ratio within the sediment layer (note that the mesh is illustrated schematically, and a much finer discretization is required for the actual analysis).

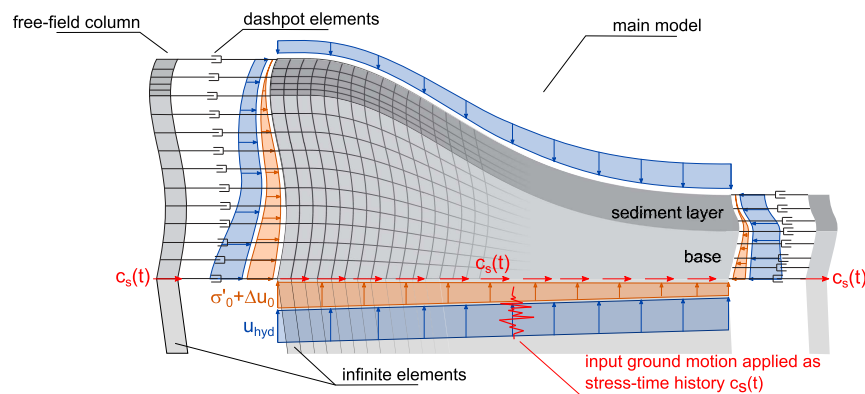


**Fig. 6.** Illustration of the plane strain finite element model for the seismic analysis (note that the mesh is illustrated schematically, and a much finer discretization is required for the actual analysis).



(Nielsen 2014). The horizontal layering, material properties, and initial conditions of the columns are identical to the adjacent parts of the main model. At the truncation boundary, a compliant base boundary condition was used (Zienkiewicz et al. 1989). The latter allows for the application of input ground motions to the model at the base while absorbing outgoing waves at the same time, thus preventing their reflection back into the model. This is achieved by connecting infinite elements to the lower boundary of the model base, which is assumed to behave elastically. Furthermore, the input ground motion is prescribed as a stress-time history, rather than applying the acceleration directly as a kinematic boundary condition. The magnitude of the prescribed stress-time history is computed as

$$c_s(t) = 2v_{su}(t)\sqrt{\rho G} \quad (3)$$

where  $\rho$  = the bulk density;  $G$  = shear modulus of the base; and  $v_{su}(t)$  = particle velocity of the upward propagating wave, i.e., half the “outcrop” motion (Mejia and Dawson 2006). The factor of 2 is required as half of the applied stress is absorbed by the viscous infinite elements.

**Termination of the analysis:** As a result of the seismic excitation of the slope, the sediments are subjected to fast, essentially undrained, cyclic loading in addition to the static loads. Sufficiently strong seismic loading can cause cyclic shear strength degradation to such a degree that the slope becomes unstable under gravitational loading, leading to rapidly increasing deformations within the unstable part of slope (i.e., a self-driven failure). Hence, the seismic analysis is terminated before a significant loss of accuracy occurs due to excessive mesh distortion, and the simulation of the mass movement is continued in the postfailure analysis. The point in time where the analysis is terminated was chosen such that two conditions are fulfilled: (1) the slope failure is already self-driven under gravitational loading (otherwise, the motion would halt in the postfailure analysis); and (2) the shear deformations and hence the mesh distortion remain within an admissible range (a threshold value of  $\Delta\varepsilon_s < 0.25$  was used here, which was reached first within the weak layer in the steepest part of the slope). At this point, the resulting stress and velocity fields (i.e., the internal strain and kinetic energy) are transferred to the subsequent postfailure analysis step.

### Step 3: Postfailure Analysis

In the postfailure analysis step, the motion of the collapsing soil mass is simulated until its final arrest. In this process, the soil undergoes large deformations, making traditional Lagrangian FE analysis techniques unsuitable to analyze the problem. Therefore, an explicit coupled Eulerian Lagrangian (CEL) FE analysis approach is employed for simulating the postfailure motion. This technique allows for materials to undergo extreme straining without suffering from excessive mesh distortion accompanied with a loss of accuracy. The approach was successfully applied to model postfailure processes of submarine landslides in several studies (Dey et al. 2016a; Trapper et al. 2015). The modeling procedure applied in this study is described in detail by Stoecklin et al. (2021) and is subsequently briefly outlined.

The CEL FE analysis technique comprises a traditional Lagrangian timestep, followed by a remap step that maps the solution from the distorted Lagrangian mesh on to the spatially fixed Eulerian mesh (Benson 1992). The material flow between neighboring elements is computed and tracked by its volume fraction, allowing for multiple materials to move within the specified Eulerian domain. In this framework, three materials were used, i.e., soil material, base material, and water (Fig. 7). The latter plays a

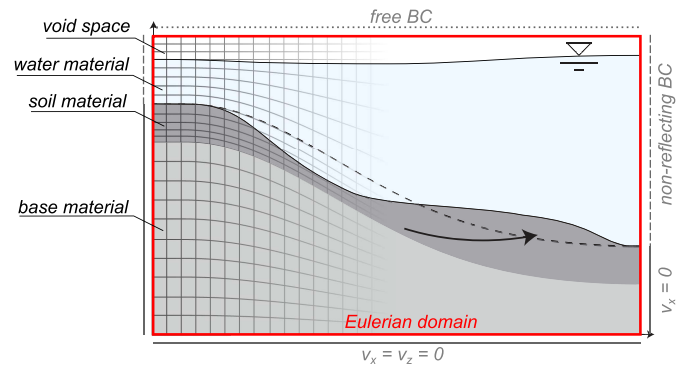


**Fig. 7.** Illustration of the CEL FE model for the postfailure analysis (note that the mesh is illustrated schematically, and a much finer discretization is required for the actual analysis). [Used with permission of Emerald Publishing, from “Controlling factors for post-failure evolution of subaqueous landslides,” A. Stoecklin, P. Trapper, and A. M. Puzrin, *Géotechnique*, Vol. 71 (10), © 2021; permission conveyed through Copyright Clearance Center.]

significant role for the postfailure motion through the effect of hydroplaning, where water gets trapped below the moving soil mass (e.g., Mohrig et al. 1998).

**Initial and loading conditions:** The initial total stress, velocity, and density fields as well as the degraded undrained shear resistance are mapped from the seismic analysis at the stage where the latter is terminated and prescribed as starting conditions for the postfailure analysis. As in the seismic analysis, gravitational loading was applied as an instant vertical acceleration to the whole model.

**Boundary conditions:** The velocities are constrained at the truncation boundary and at the lower lateral boundaries, where soil material is present (see Fig. 7). Nonreflecting boundary conditions were applied at the lateral boundaries of the water body to reduce the effect of reflecting pressure waves (Dassault Systèmes 2014). A void space was included above the water surface. The out-of-plane component of the velocity was set to zero to enforce plane-strain conditions.

### Computational Meshes

For the sedimentation analysis, the required mesh size is mainly determined by fluid flow and the large volumetric deformations of sediments. For the seismic analysis, on the other hand, the propagation of seismic stress waves as well as the formation of a localized basal shear band need to be captured accurately. Further on, for the postfailure analysis the discretization has to be fine enough to capture the propagation of the localized shear bands and the large shear deformations of the collapsing sediments. Furthermore, different element types were used in each analysis step, i.e., bilinear plane strain Lagrangian elements in the sedimentation and the seismic analysis and a single plane of eight-node 3D continuum reduced integration Eulerian elements for the postfailure analysis. Hence, each analysis step requires a different level of discretization to capture the governing effects with sufficient accuracy. In this study, however, a constant number of elements with an element size of  $h_{EL} \approx 0.5$  m was used in all analysis steps to simplify the mapping of the stress, density, and velocity fields between steps. This element size corresponds to the minimum value of the required element size of all three analysis steps, which was governed here by the postfailure analysis. To ensure the equilibrium of the prescribed initial stress field, the initial mesh configuration for the



seismic and postfailure analyses correspond to the deformed configuration of the updated Lagrangian, large deformation sedimentation analysis. To improve the efficiency of the simulation, this could be improved in future studies by remapping the analysis results between steps onto different computational meshes.

## Description of the Constitutive Soil Behavior

As outlined in the previous section, different processes and thus different material properties govern the behavior of the landslide during the analyzed stages:

1. During the sedimentation process, the soil undergoes large volumetric compaction along with a drastic change in stiffness, hydraulic conductivity, and density. Hence, the consolidation behavior of the soil is of primary importance.
2. During the seismic excitation, the soil is subjected to fast, cyclic loading, making the undrained hysteretic stress–strain behavior under combined static and cyclic loading a crucial factor.
3. In the postfailure stage, the soil undergoes large straining and shear deformation. Therefore, an accurate representation of the undrained stress–strain behavior at large deformations becomes crucial for the outcome.

To illustrate the stress history throughout the landslide evolution, a typical stress-path at a point within the model is shown in Fig. 8. The sediments undergo consolidation during the sediment deposition, followed by undrained, cyclic loading during the seismic analysis and essentially monotonic shearing during the post-failure analysis. Ideally, the soil behavior would be represented using one single constitutive model throughout the entire evolution, capable of accurately capturing all the aforementioned properties. However, to the authors' knowledge, no such constitutive model exists that is also readily applicable and implementable for all the applied FE methodologies. Therefore, different constitutive models are applied to accurately represent the governing aspects of the soil behavior in each step. The constitutive models are chosen such that the strength and elastic stiffness definitions are consistent throughout the simulation, facilitating the transferring of the stress-fields between the different analysis steps. Subsequently the constitutive behavior of the soil and the derivation of the simulation input parameters are described for the different simulation steps.

### Sedimentation Analysis

In the sedimentation process, soil particles are deposited on the lake bottom in a loose state with a very high initial water content. As the deposited sediments get buried over time, they consolidate with the overburden and their mechanical properties change. Hence,

intrinsic mechanical soil properties (i.e., soil properties that are assumed to remain constant during compaction) are used to model this process as well as initial state parameters (such as the initial void ratio  $e_0$  of the sediments near the seafloor after deposition). The change of the mechanical properties over the height of the soil profile is then an outcome of the analysis. The constitutive behavior of the sediments was modeled using the modified cam clay (MCC) model (Roscoe and Burland 1970), as it captures the strong increase in volumetric stiffness with advancing consolidation (i.e., the logarithmic relation between the void ratio  $e$  and the mean effective stress  $p'$ ) as well as the contractive behavior of normally consolidated soils during shearing. The derivation of the required input parameters for the analysis of the cases is described in Appendix I.

### Seismic Analysis

During seismic loading, the soil is subjected to a combination of the sustained, gravitational static and fast, cyclic loading. Under such loading conditions, the soft, normally consolidated sediments typically experience a buildup of excess pore water pressures along with a degradation of stiffness and strength. In the case of sufficiently severe cyclic loading, the shear resistance of the soil can degrade below the gravitational stress demand, resulting in a self-driven, catastrophic failure of the sediment layer. To capture this behavior, the sediments' constitutive behavior is represented by a multisurface kinematic hardening model (Montáns 2001; Prevost 1985; Stoecklin et al. 2020). The applied model is intended to represent the behavior of normally consolidated, fine-grained soils under undrained cyclic loading conditions. The conceptual response of the constitutive model is depicted in Fig. 9. As a result of the multiple frictional kinematic hardening surfaces, the stress–strain response is nonlinear in virgin loading as well as in un- and reloading. The higher the mobilized shear stress, the more yield surfaces become active, resulting in a larger plastic strain component and a lower deviatoric stiffness. Similarly, the volumetric flow rule on each surface causes a contraction of the soil during yielding, causing the buildup of excess pore pressures under undrained loading conditions with each loading cycle. This pore-pressure buildup continues, until a critical state is reached [Point C in Fig. 9(a)].

Since the constitutive model is only applied to simulate the undrained stress–strain response during seismic loading, where the effective stress decreases due to the pore pressure buildup, a volumetric cap would remain inactive and is not included. Due to the Drucker–Prager-type yield surfaces, the failure definition is consistent with the MCC model, allowing the mapping of the initial stresses from the preceding sedimentation analysis. The sustained,

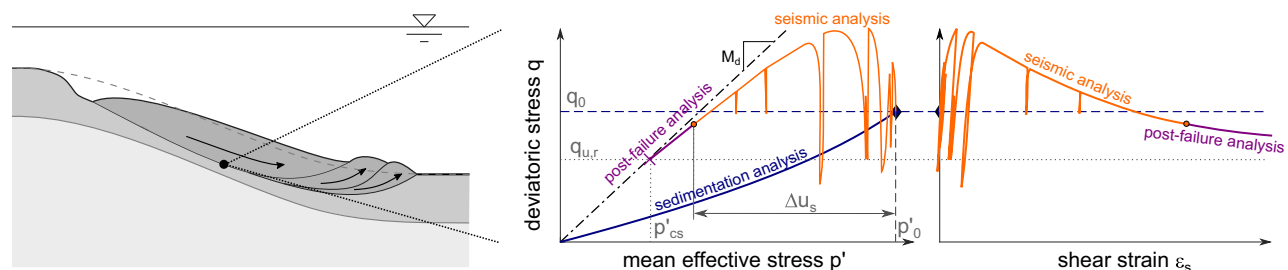


**Fig. 8.** Illustration of the computed stress-path for a single point within the slope throughout the simulation: During the sedimentation process, the soil undergoes consolidation along with an increase in the effective stress. When an earthquake occurs, undrained cyclic loading of the soft sediments leads to a buildup of excess pore water pressures along with a weakening of the sediments. At some stage, the shear resistance is degraded below the static stress demand, and the slope-failure becomes self-driven as the stress path softens toward the remolded shear resistance.

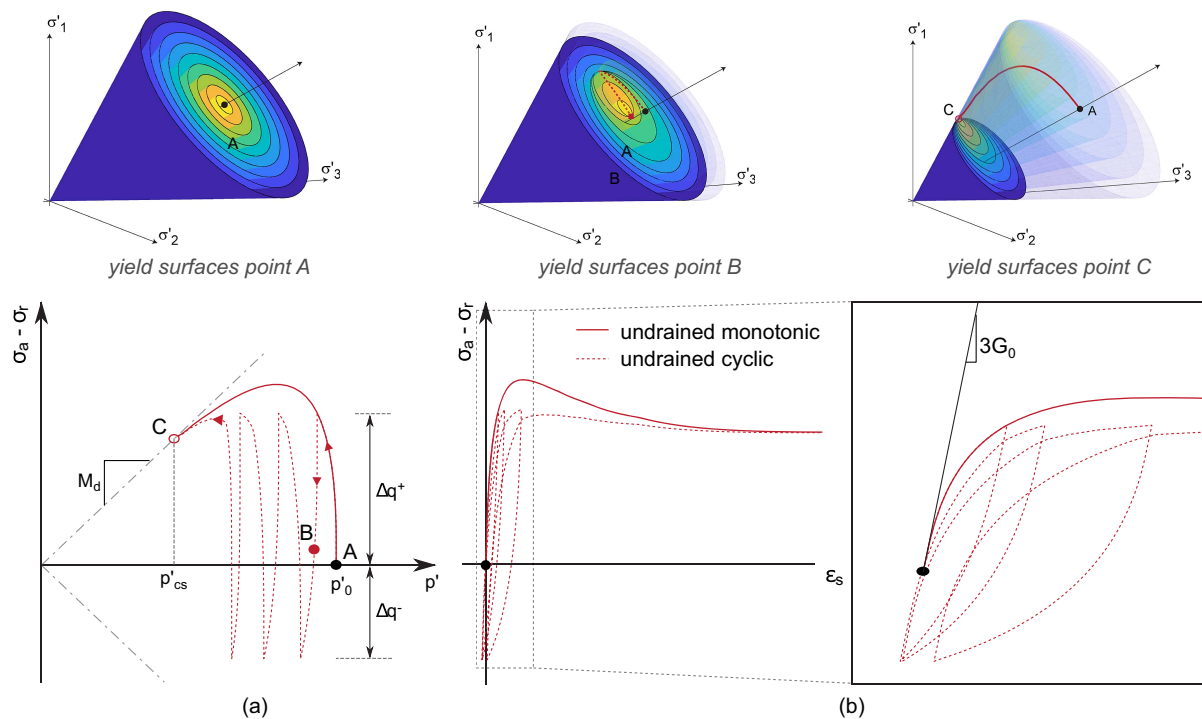


**Fig. 9.** Illustration of the multisurface kinematic hardening model response for an element test under triaxial loading conditions: (a) shows the predicted effective stress-path; and (b) the deviatoric stress–strain curve. [Used with permission of John Wiley Sons, from “A multisurface kinematic hardening model for the behavior of clays under combined static and undrained cyclic loading,” A. Stoecklin, B. Friedli, and A. M. Puzrin, *International Journal for Numerical and Analytical Methods in Geomechanics*, Vol. 44 (17), © 2020; permission conveyed through Copyright Clearance Center.]

static shear stress on the slope prior to the undrained loading can have a significant effect on the undrained shear resistance (e.g., Ladd and Edgers 1972). To account for this effect on the undrained stress–strain response, the yield surfaces are shifted toward the consolidation stress in their initial configuration. The model is formulated in effective stress-space but implemented for total stress-based implicit analyses, assuming fully undrained conditions. More details on this and the model formulation in general is provided by (Stoecklin et al. 2020). The required input parameters and their derivation for the analyzed cases are described in Appendix II.

### Postfailure Analysis

In this analysis step, the soil is subjected to large shearing deformation. Hence, the stress–strain behavior up to large deformations is of particular importance. At the same time, the applied constitutive model has to be applicable for the applied CEL FE analysis technique, which does not allow for the use of anisotropic material behaviors. To satisfy these conditions, a constitutive model with a van Mises-type failure envelope and isotropic strain softening was used to describe the undrained deformation behavior of the sediments. The stress–strain curve is linear and elastic up to the peak shear strength, followed by linear strain softening until the remolded value is reached and the strength remains constant. The degraded peak and the remolded van Mises shear strength were computed from the results of the preceding analysis steps for each integration point as

$$q_{u,p} = M_d \cdot (p'_0 - \Delta u_s) \quad (4)$$

$$q_{u,r} = M_d \cdot p'_{cs} \quad (5)$$

where  $M_d$  = the inclination of the failure surface;  $p'_0$  = mean effective consolidation stress from the sedimentation analysis;  $\Delta u_s$  = excess pore pressure generated during undrained seismic loading; and  $p'_{cs}$  = parameter defining the remolded undrained shear resistance (see Fig. 8).

To avoid a significant mesh dependency of the results due to the strain softening behavior, a simplified scaling rule was applied, wherein it is assumed that the shear-band occurs within a single element. The plastic shear strength, at which the material is fully softened, was defined as a function of the residual shear displacement  $\delta_r$  and scaled with the element size  $\varepsilon_{s,r}^p = \delta_r / \sqrt{3}h_{EL}$  (Dey et al. 2015, 2016b; Stoecklin et al. 2021). The same approach was applied for the seismic analysis. The water was modeled as a nearly incompressible, viscous Newtonian fluid using an equation of state model (Trapper et al. 2015). The derivation of the additional soil parameters for the analysis of the case studies is described in Appendix II.

### Analysis of the Case Studies

In this section, the results from the simulation of the Zinnen slides and the Oberrieden Slide are presented. In a first step, a simplified and computationally more efficient 1D analysis was performed to investigate the triggering of the selected cases and the effect of the input ground motion on the seismic response of the slopes. In a second step, the full landslide evolution was simulated for the selected cases. For all simulations, the same sets of parameters were used, which are listed in Tables 1 and 2 in Appendixes I and II.

### Simplified 1D Analysis of the Triggering Process

In a first step, a simplified infinite slope analysis was conducted to investigate the seismic response of the two slopes when subjected to different ground motions. The methodology, as outlined in the previous section, was applied, but the simplified 1D model consists only of a single column of elements to minimize the computational cost [see Fig. 10(a)]. For each analysis run, the slopes were subjected to a different input ground motion to gain insight into the effect of different ground-motion characteristics on the stability of the slopes. A total of 100 time-histories with a peak spectral acceleration of  $PSA < 1$  g were randomly selected from a set of representative ground motions for Switzerland (Laue 2014). The moment magnitudes of the applied ground motions vary between 4.3 and 6.6. The magnitudes of the seismic events that are believed to have triggered the analyzed cases lie within this range.

For each of the simulations, it was evaluated whether the slope remained stable under static conditions after the earthquake event or whether the ground motion triggered a self-driven failure of the slope. Failure of the slope was said to occur if the shear strength of the sediments is degraded below the gravitational shear stress at any horizon within the soil deposit during the earthquake event. This is illustrated for the Oberrieden Case in Fig. 10, where results of two exemplarily simulation runs are shown, i.e., a case where the ground motion triggered a slope failure and another where the slope remained stable. From the stress paths, it can be observed that slope failure occurred, where the cyclic loading led to a significant buildup of excess pore water pressure and degradation of the shear resistance below the gravitational shear stress ( $\tau_g$ ) [Fig. 10(b)]. In the other case, the buildup of excess pore water pressure during cyclic loading  $\Delta u$  is not significant enough to cause the degradation of the shear strength below the gravitational shear stress, and the slope remains stable under static conditions after the earthquake event [Fig. 10(c)].

The simulations for the selected 100 input ground motions were performed for the Zinnen Slide and the Oberrieden Slide settings: an average slope gradient of  $\alpha = 25^\circ$  and a thickness of the soil deposit of  $H \approx 6$  m were chosen to represent the Zinnen Slope, and  $\alpha = 12^\circ$  and a  $H \approx 7$  m for the Oberrieden Slide 2, respectively (see Fig. 11). The results show that the various input ground motions have different impacts on the stability of the slopes. Whereas some ground motions only cause minimal irreversible deformations in the slope, others trigger a catastrophic failure within a few seconds of strong ground motion. The results indicate that there does not seem to be a clear correlation between typical ground motion characteristics, such as peak acceleration, peak velocity, or peak spectral acceleration and the impact of the ground motion on the stability of the slope. However, it can be observed that ground motions with a higher energy content at lower frequencies had a much more damaging effect on the slopes. This is depicted in Fig. 11, where the elastic response spectra of the ground motions that triggered a slope failure and those for which the slope remained stable are shown. Failure of the Zinnen Slope was predicted for most ground motions with significant energy content at higher periods [see Fig. 11(a)], whereas the Oberrieden Slope remained stable under the impact of all but four of the 100 applied ground motions [see Fig. 11(a)]. This difference can be explained by the different slope angles. Nonetheless, the more damaging effect of the time histories with high energy content at higher periods on the slope was observed for both cases. In the following section, the results of the 2D analyses are presented, where the input ground motion RSN 388 was applied to trigger the slope failure.

### 2D Analysis of the Zinnen Slides

For the Zinnen slides, the deposition of the sediment layer on the sloping ground at an average sedimentation rate of 0.4 mm/year (Strasser and Anselmetti 2008) was simulated in a first step,

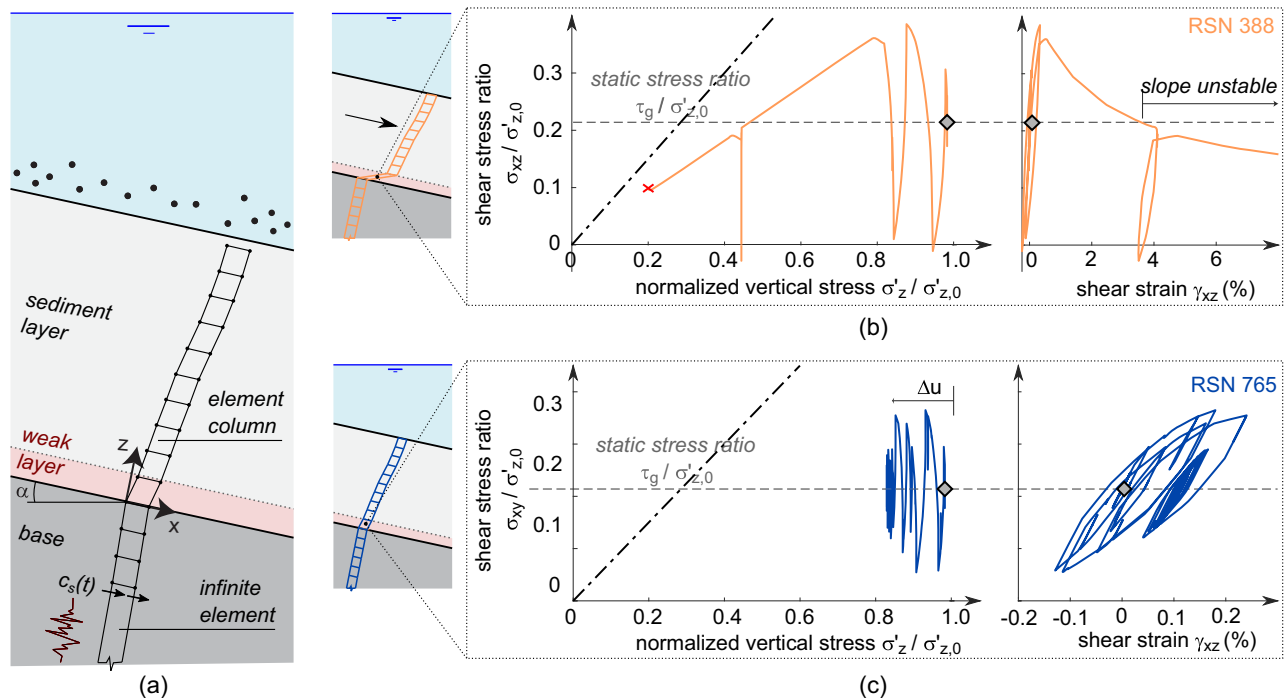


**Fig. 10.** Simplified 1D analysis of the Oberrieden Slide 2: (a) illustration of the 1D model; (b) effective stress path and stress–strain path from an exemplary simulation run where slope failure was triggered by the earthquake motion; and (c) of an exemplary simulation run where the slope remained stable.



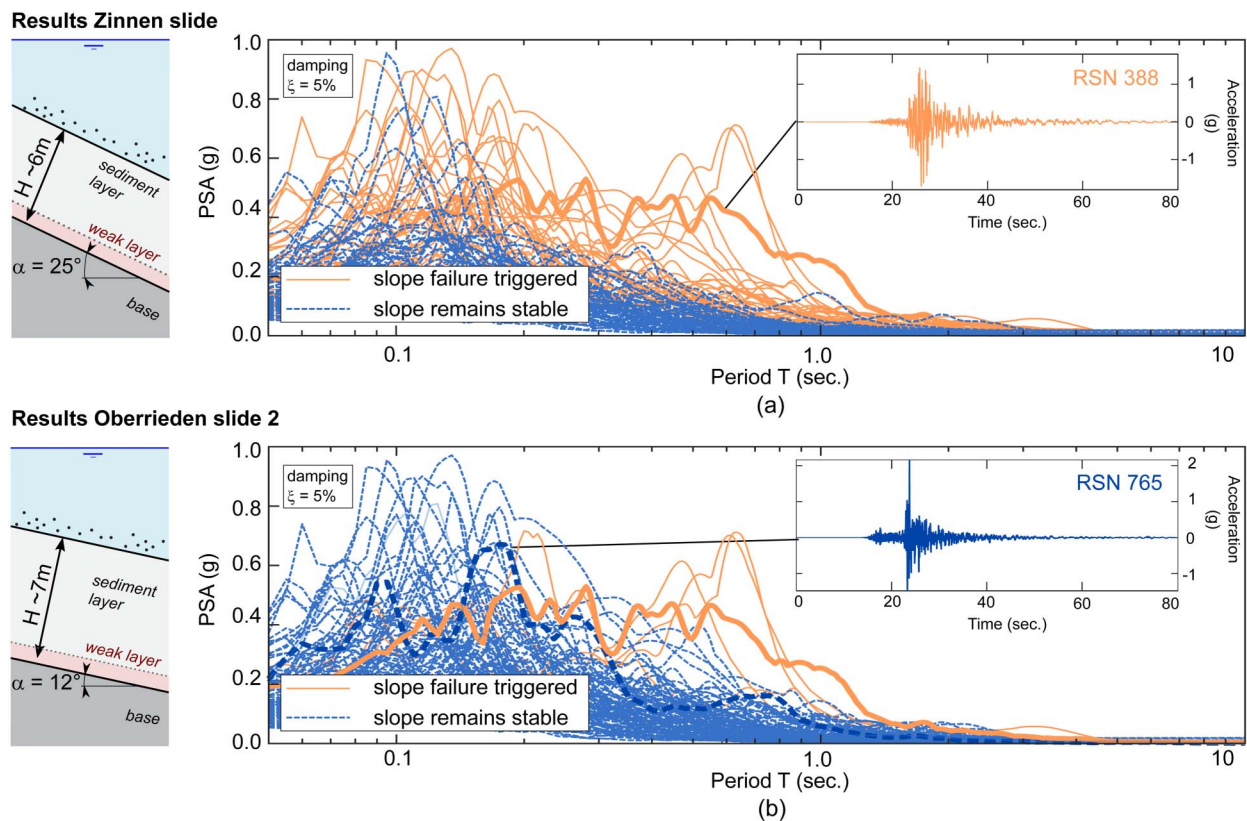


**Fig. 11.** Effect of different ground motions on the stability of the slopes: elastic response spectra of the applied time-histories, which triggered a slope failure (solid line), and of those for which the slope remained stable (dotted line) for (a) the Zinnen; and (b) the Oberrieden slide.

providing a prediction of the prefailure stress and density field within the sediments. The resulting overpressures are small, resulting in nearly normally consolidated prefailure soil profiles. Applying the earthquake ground motion (RSN 388) to the slopes caused a significant degradation of the sediment shear resistance and the initiation of the slope failure. Hence, the seismic analysis was terminated after a few seconds of ground motion and the results transferred to the postfailure analysis, where the self-driven motion of the mass movement was computed. The simulation results of the 2D analysis of the two Zinnen slides are illustrated in Fig. 12, where different stages of the failure process are depicted.

In both simulations, the shear band is first initiated by the ground excitation and propagates quickly into the stable zone in the basin. The unstable sediments above the basal shear zone accelerate and move downward toward the toe of the slope, where they thrust into the stable basin sediments, causing a disturbance of the basin sediments. Subsequently, the unstable soil mass emerges and moves over the soft and weak sediments near the lake bottom until the displaced mass is at rest again. This same failure pattern was observed for the Zinnen Main and the Zinnen Baby Slide. However, as a consequence of the thicker sediment deposit, the main slide propagates further into the basin, leading to a larger runout distance.

In Fig. 13, the computed slide deposit is compared with seismic reflection profiles recorded along the deposits of the Zinnen Main and the Baby Slide, which were published by Sammartini et al. (2021). It should be mentioned that the seismic reflection profiles were not recorded at the exact location where the cross section for the analyses was taken but in the vicinity. The plotted plastic strain contours in Fig. 13(a) show that the basin sediments are disturbed near the toe of the slope to a greater depth, which decreases

with increasing distance from the slope. The basal shear bands propagated along the weaker layer in the lower part of the sediment deposit at the transition between the Holocene and late glacial unit. These observations are consistent with the interpretation of the recorded seismic profiles by Sammartini et al. (2021). Further, the predicted deformation front (i.e., tip of the displaced soil material) can be compared with the field observation [i.e., the distinct frontal thrust, dividing the slide deposit from the undisturbed basin strata (Sammartini et al. 2021)]. For the Main Slide, it is slightly under-predicted, whereas for the Baby Slide slightly over-predicted. Nonetheless, the overall prediction matches the observed deformation front in the field rather well. The extent of the mobile mass-flow deposit, on the other hand, exceeds the extent of the model prediction, particularly for the Zinnen Baby Slide. This can be attributed to the fact that the soil and water are treated as two separate materials, without accounting for entrainment and mixing of the two materials (see section on limitations).

### 2D Analysis of the Oberrieden Slide 2

For the Oberrieden Case, the deposition of the sediment layer on the sloping ground was simulated with an average deposition rate of 0.5 mm/year (Strasser et al. 2013), resulting in a nearly normally consolidated soil profile due to the relatively slow sedimentation rate. Applying the earthquake ground motion (RSN 388) to this slope for about 10 s of strong ground motion initiated a self-driven slope failure. At this stage, the results were transferred to the postfailure analysis, where the self-driven motion of the mass movement was computed until its final arrest. The resulting velocity of the moving soil mass is depicted in Fig. 14(a) for different stages throughout the failure process. The predicted velocities

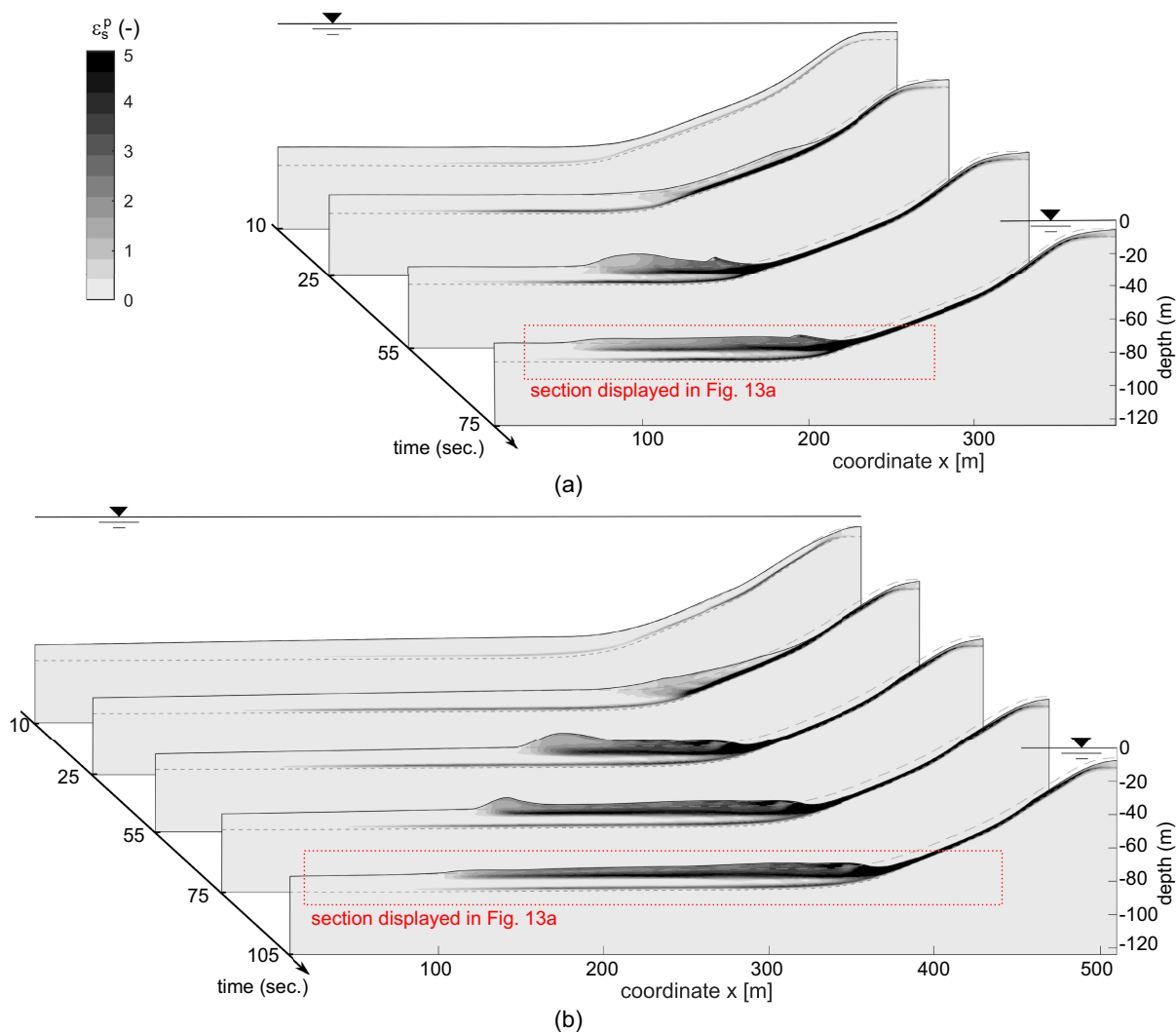


**Fig. 12.** 2D analysis of the slope failure process of the two Zinnen slides: (a) evolution of the computed plastic shear strain ( $\epsilon_s^p$ ) at different points in time for the Zinnen Baby Slide; and (b) for the Zinnen Main Slide.

increase as the unstable soil mass glides down the steeper parts of the slope, reaching a maximal speed of about 6.5 m/s. As the moving soil mass reaches the toe of the slope and moves over the stable plane Basin sediments, it decelerates slowly until arrest. The predicted geometry of the final slide deposit is compared with the in situ lake bottom, as shown in Fig. 14(b). The simulation provides a good match of the runout distance. The slide head scarp, on the other hand, is predicted further upslope than the observed head scarp.

The model prediction is compared directly with the present in situ bathymetry, neglecting changes in the deposits during the landslide event and the present. Since the postfailure sediment drape of about 10 cm (Strupler et al. 2017) is small compared with the thickness of the slide deposit, this can be justified.

## Discussion of the Results

### On the Model Framework and Its Limitations

The main hazard imposed by subaqueous landslides arises from the destructive movement of the unstable soil mass in the postfailure stage. Yet, the landslide kinematics can be influenced by various

processes at earlier stages, affecting the slope stability before a collapse occurs. The presented modeling framework allows for the simulation of this continuous process in a consistent manner, ranging from sediment deposition to seismic triggering to the postfailure evolution. It facilitates investigating the role of sedimentation as a long-term preconditioning process and seismic shaking as a triggering process on the postfailure dynamics of slope failures. To model the governing processes in each step, such as fluid flow during sediment deposition, stress-wave propagation during seismic excitation and the large deformation of the sediments during the slope collapse, different methodologies are applied. Finding a balance among the accuracy, complexity, and applicability of the approach presents a challenge and requires trade-offs. In this study, an attempt was made to include what the authors consider the governing effects, while making some simplified assumptions in other areas, in order to keep the framework and the parameter derivation lean. As a result, there are a number of limitations, which should be kept in mind when applying the framework and interpreting the results.

- Constitutive behavior: The nonlinear, degrading, and hysteretic stress–strain behavior of the sediments during combined gravitational and seismic loading was represented by a multisurface kinematic hardening model (Stoeklin et al. 2020). While the

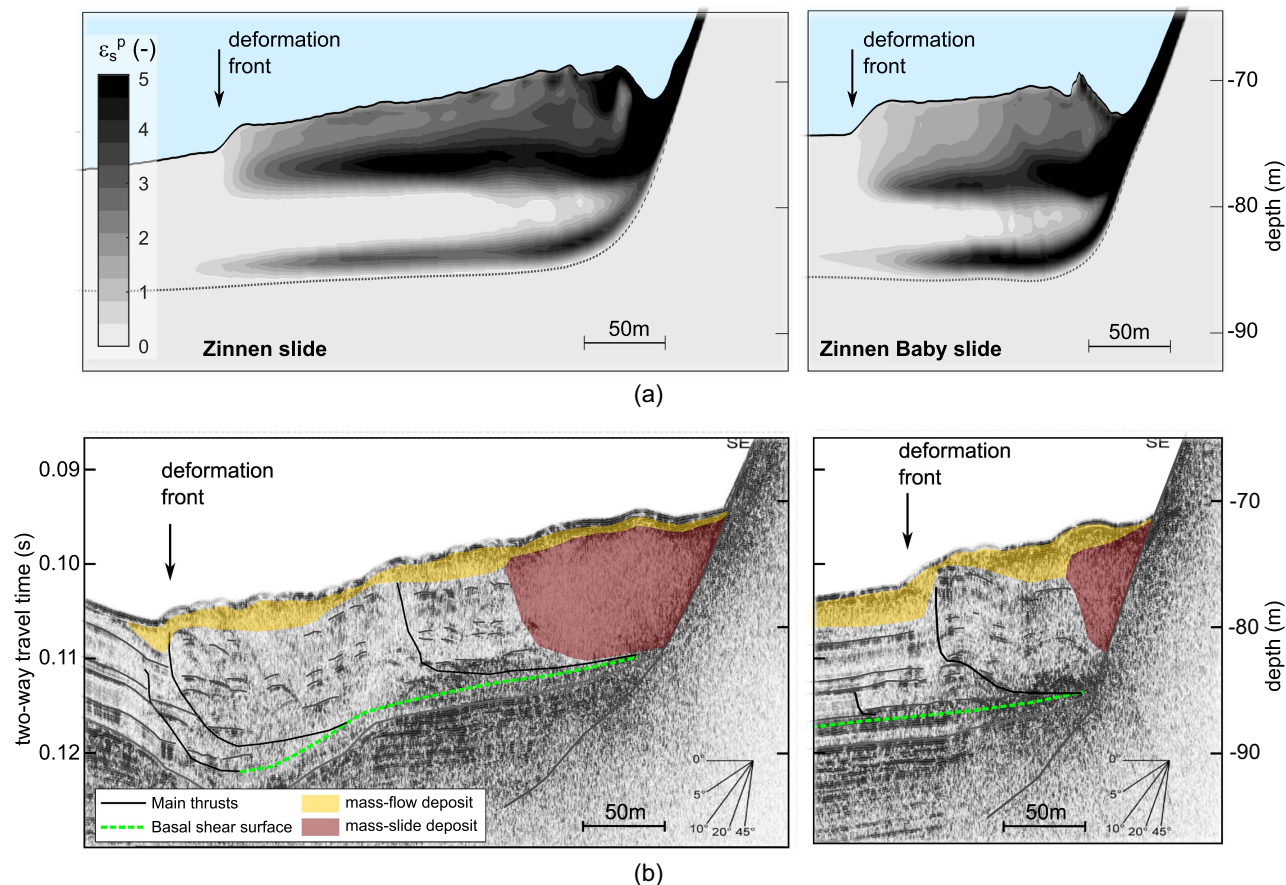


**Fig. 13.** Comparison of the predicted and the observed Zinnen slide deposits: (a) computed plastic shear strain contours for both the Zinnen Main Slide (left) and the Baby Slide (right); and (b) corresponding sections of seismic reflection profiles through the slide deposits [reproduced from Sammartini et al. (2021), under Creative Commons-BY-4.0 license (<https://creativecommons.org/licenses/by/4.0/>)].

constitutive model accounts for many aspects, which are considered important for the seismic response of slopes, it does not include rate effects. Hence, a calibration of the strength parameters corresponding to a representative rate is required. Furthermore, while the model is formulated in effective stress space, it is implemented for total stress-based FE analysis, neglecting fluid flow and redistribution of pore water pressures during the earthquake event. While this effect is not considered significant for the analyzed cases, it limits the applicability of the model to co-seismic triggering analyses. Simulating delayed, postseismic slope failures due to creep (e.g., Andersen 2015), would require a constitutive model that captures rate-dependent soil behavior.

- Application of the ground motion: The ground motion is applied as a uniform stress time history at the base of the model, implying that the earthquake signal arrives at the same time along the entire base. This may lead to inaccuracies when analyzing long-stretched slope geometries. This shortcoming could be overcome by embedding the FE model into a larger model, which simulates the earthquake source and propagation path (e.g., Bielak 2003).
- 3D geometrical effects: The analyzed landslides are relatively uniform in the lateral extent, thus justifying the presented 2D plane strain analysis. Many slides, however, show more complex geometries, thus requiring a more complex full 3D analysis. To simulate mass movements on more complex terrain, the presented framework could be extended to model slope geometries in three dimensions. This would require introducing

free-field planes at the lateral boundaries in addition to the free-field columns for the seismic analysis (e.g., Nielsen 2014). Apart from that, the procedure could be applied as is for full 3D analyses.

- Turbidity currents and highly mobile mass flows: A shortcoming of the applied CEL approach to model the postfailure stage is the separation of the water and the soil material. Whereas the principal effect of hydroplaning can be captured with the procedure (Stoecklin et al. 2021) (although it was not observed for the cases analyzed in this study), the method does not account for the entrainment and mixing of water within the moving soil mass. Hence, the remolded strength of the soil is defined solely as a function of the initial consolidation stress after the sedimentation analysis. Landslides, which transform into long runouts, however, entrain water and can evolve into fluidlike turbidity currents (e.g., Randolph and Gourvenec 2011). Predictions with the presented procedure would therefore likely underestimate the runout distance for such slides. Nonetheless, for the initial sliding phase, where the landslide deforms as a continuum along localized shear bands, the effect of water entrainment is considered to be small. The procedure could be extended in the future to include the effect of water entrainment and simulate the transition of slope failures into turbidity currents.

### On the Analyzed Case Studies

Aspects of the obtained results from the analyses of the Oberrieden and Zinnen slides are discussed as follows:



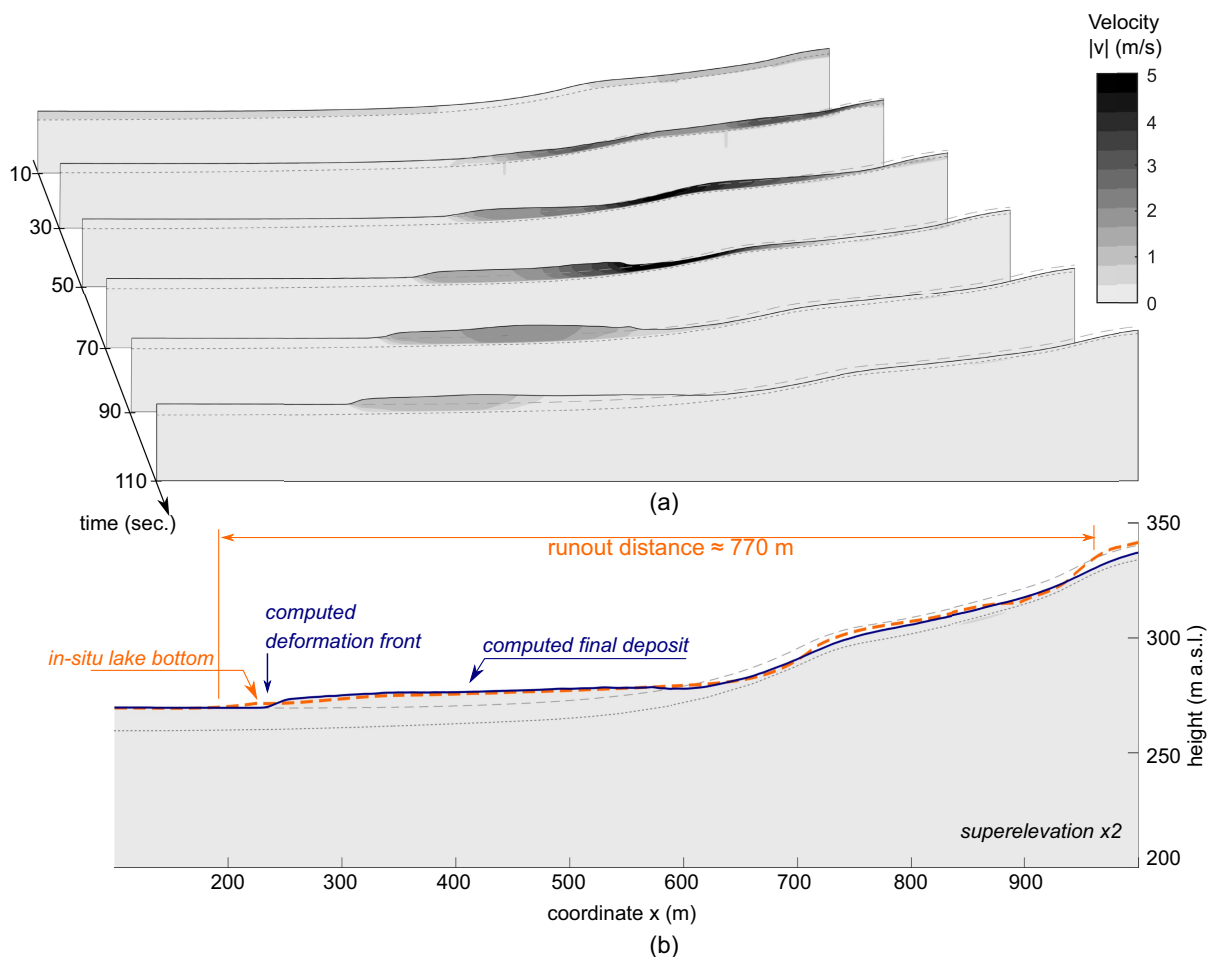


**Fig. 14.** Results of the 2D analysis of the Oberrieden Slide 2: (a) velocity contours at different time points during the failure evolution; and (b) comparison of the predicted and in situ geometry of the slide deposit.

- **Sedimentation:** The simulation results show that overpressures due to sedimentation are not significant for the analyzed cases. Hence, the sedimentation analysis could also have been replaced by a simpler drained, static analysis step in this case. Nonetheless, the sedimentation analysis provides accurate initial conditions for the subsequent analysis steps, including the consolidation history of the sediments and the strong variation in density and stiffness of the sediments within the deposit.
- **Seismic triggering:** The geomorphological site investigations suggest that the analyzed historical slope failures were most likely triggered by earthquakes (Sammartini et al. 2021; Schnellmann et al. 2005; Strupler et al. 2017). The results from this study show that different ground motions affected the stability of the slopes to different degrees. The results suggest that PGA and PSA alone do not reflect the detrimental effect of an earthquake event and that the frequency content of the ground motion is a more significant ground motion characteristic for the assessment of the slope stability. The ground motions with lower frequency contents affected the stability of the analyzed slopes much more than those with higher predominant frequencies. These results are in agreement with findings by Biscontin and Pestana (2006), who investigated factors affecting the response of submerged slopes under seismic loading. Cyclic loading at frequencies well below the natural period of the system result in long loading cycles and nearly quasistatic loading of the slope, causing high shear stresses in the weak layer.

This appears to have a particularly damaging effect on the slope compared with loading at higher frequencies, where parts of the sediment layer above the weak layer are moving in one direction, while other parts are moving in the opposite direction, thus limiting the relative stress demand at the depth of the weak layer. Although these findings are limited to the analyzed cases, the results highlight the complexity of the seismic triggering process and the challenge of predicting the stability of slopes using quasistatic analyses, where the horizontal acceleration is typically related to ground motion characteristics. The results further show that not all ground motions initiate a failure of the slopes. Exposure to repetitive excitation of this type could have a strengthening effect on the stability of the slope, if sufficient time remains for excess pore water pressures to dissipate between seismic events. This effect of seismic strengthening has been observed in areas of frequent seismic activity and low sedimentation rates (ten Brink et al. 2016; Sawyer et al. 2017; Sawyer and Devore 2015; Strozyk et al. 2010). By adapting the presented approach to simulate the effect of repetitive ground excitation with intermittent redistribution and dissipation of excess pore water pressure, this effect could be further investigated in the future.

- **Prediction of the landslide deposit:** As most often, no direct measurements of the actual landslide event are available for the analyzed cases, which is why the model predictions were validated against the in situ geometry of the landslide deposits.

Overall, the simulation provided a good prediction of the landslide deposit and the deformation front without backcalibration of the input parameters. However, it should be mentioned that not enough test data were available to calibrate all input parameters from direct measurements. Whereas some parameters, such as the undrained shear resistance, were calibrated directly against measurements on intact sediments adjacent to the landslide areas, other parameters, such as the sediment sensitivity, the stiffness degradation, or cyclic shakedown parameters, were derived using correlations and test data from similar soils. In particular, the estimation of the sediment sensitivity, one of the controlling parameters for the predicted runout distance (Stoecklin et al. 2021), results in a significant uncertainty of the model predictions. Due to a lack of direct measurements for the analyzed sites, this parameter was derived from investigations at nearby sites with a similar lithology (see Appendix II). The outlined parameter derivation procedure therefore serves as a first-order approach. The simulation results serve as a validation of the general model behavior and illustration of principal effects rather than a detailed hazard assessment of the sites. The latter would require a more extensive site characterization.

- Applicability of the framework for hazard assessments: The presented results are site-specific and should therefore not be extrapolated generally for hazard assessments of underwater slopes. Furthermore, the model predictions have, thus far, only been validated against historical slides in rather specific alpine settings. In future studies, the procedure should therefore be validated against a wider range of mass movements in a wider range of settings to assess the accuracy of the predictions and the model limitations more broadly. This could provide further insight into the controlling factors for the kinematics of subaqueous landslides. One particularly useful application of the framework lies in the assessment of landslide-induced tsunamis. Underwater landslides are a well-known source of tsunamis in marine (Fine et al. 2005; Fryer et al. 2004; Tappin et al. 2001) and lacustrine environments (Schnellmann et al. 2002; Strasser et al. 2007). As highlighted in a recent study by Løvholt et al. (2017), the strength of landslide-induced tsunamis is closely related to the slide failure mechanism and that similarly sized slides can produce very different tsunamis. By extracting the moving boundary between the soil and the water over time, the simulation results could provide an accurate source input for subsequent tsunami propagation modeling.

## Conclusions

Investigations of historical landslide events have revealed that various processes, acting on different time scales, can play a role in the formation and evolution of underwater landslides. Predicting future landslide events and their behavior therefore remains a challenging task. In this study, a modeling framework is presented, which facilitates the simulation of subaqueous landslides as an evolving process in a sequence of steps, ranging from sediment deposition, to seismic triggering to postfailure evolution of the collapsing soil mass. Different FE-based methodologies were applied to model the governing processes and specific particularities for each step. The analyses of the individual steps were performed using the FE-code ABAQUS and connected in a consistent way, facilitating the mapping of results of preceding steps as initial conditions for subsequent steps and thus simulating the landslide evolution as a continuous process. This enables quantifying the effect of sedimentation and earthquake loading on the postfailure

landslide dynamics. It can thus help improve our understanding of the governing mechanisms involved in subaqueous landsliding.

The presented procedure was applied to analyze three seismically triggered, well-investigated, historical landslides in Swiss lakes, i.e., the two Zinnen slides in Lake Lucerne and the Oberrieden 2 Slide in Lake Zurich. The predicted deformation patterns match the observed landslide deposits in the field well, thus serving as a validation of the model approach and providing new insights into the failure mechanisms. The analysis of the triggering process showed that excitation of the slopes by various ground motions affected the stability of the slopes to varying degrees. The ground motions with high energy content at low frequencies generally appeared to have the most severe effect on the stability of the analyzed slopes.

The presented framework is focused on the modeling of the most commonly cited preconditioning (rapid sedimentation) and triggering factor (earthquake events) of subaqueous slope failures. However, many more processes are known to influence the stability of slopes, such as gas hydrate dissociation, groundwater flow, sea-level changes, groundwater seepage, storm-wave loading, and human activity. To investigate the impact of such processes, the framework could be extended in the future by joining additional steps or replacing existing ones. Furthermore, the model predictions have, thus far, only been validated against historical slides in rather specific lake settings. In future studies, the accuracy of the model predictions should therefore be validated against a wider range of mass movements in different settings. Nonetheless, the presented approach provides a basic framework for assessing and quantifying the effects of different processes involved in subaqueous mass wasting. This could further improve our understanding of the factors controlling the landslide dynamics and ultimately improve hazard assessments and the design of mitigation measures.

## Appendix I. Derivation of the Input Soil Parameters for the Static Sedimentation Analysis

Subsequently, the derivation of the required input parameters for the static sedimentation analysis of the analyzed cases is described.

- Initial void ratio  $e_0$ : The initial void ratio corresponds to the void ratio of the sediments at deposition and therefore to the value near the lake bottom. Assuming the sediments are fully saturated, the initial void ratio can be derived from the water content measured near the lake bottom  $w_0$  according to

$$e_0 = g_s w_0 \quad (6)$$

where  $g_s \approx 2.65$  = the grain specific density. At the Oberrieden (Strupler et al. 2017) and Zinnen sites (Sammartini et al. 2021), similar water content near the lake bottom of  $w_0 \approx 150\%$  was measured, resulting in an initial void ratio of  $e_0 \approx 4.0$ . The effective bulk density of the sediments near the seafloor  $\rho'_0$  is derived from the initial void ratio

$$\rho'_0 = \left( \frac{g_s + e_0}{1 + e_0} - 1 \right) \cdot \rho_w \quad (7)$$

where  $\rho_w$  = the bulk density of the pore water. The resulting void ratio and density distribution within the sediment layer are model outputs.

- Consolidation properties: The compression index  $C_c$  and swelling index  $C_s$  determine the change in stiffness with increasing compaction. For the Zinnen site, the compression index was measured as  $C_c \approx 1.7$  (Sammartini et al. 2021). For the

**Table 1.** Summary of input parameters for the sedimentation analysis

Type	Parameter	Symbol	Value (Zinnen slides)	Value (Oberrieden slides)
Permeability	Hydraulic conductivity at liquid limit	$k_L$	$2 \times 10^{-9}$ m/s	$2 \times 10^{-9}$ m/s
Initial conditions (i.e., values near lake bottom)	Initial void ratio	$e_0$	4.0	4.0
	Initial density near the lake bottom	$\rho_0$	1,330 kg/m <sup>3</sup>	1,330 kg/m <sup>3</sup>
Consolidation properties	Compression index	$C_c$	1.7	1.0
	Permeability index	$C_k$	$= C_c/1.5$	$= C_c/1.5$
	Swelling index	$C_s$	$= 0.2 \cdot C_c$	$= 0.2 \cdot C_c$
Strength properties	Inclination of the failure surface (= CSL)	$M$	1.7	0.9

Oberrieden site, a value of  $C_c = 1.0$  was assumed. For the swelling index, a typical value of  $C_s = 0.2 \cdot C_c$  was assumed.

- Hydraulic conductivity  $k$ : The change in hydraulic conductivity is computed as a function of the void ratio, using the commonly used logarithmic expression (Mesri and Rokhsar 1974; Tavenas et al. 1983)

$$e = e_0 + C_k \cdot \log_{10} \frac{k}{k_0} \quad (8)$$

where  $C_k$  = permeability change index; and  $k_0$  = initial hydraulic conductivity. In absence of direct measurements, an empirical correlation was used to determine value of  $k_0$ . Experiments have shown that, for a wide range of soils, the hydraulic conductivity at the liquid limit lies within a relatively narrow range of  $k_L = 0.13 - 2.8 \cdot 10^{-9}$  m/s (Mitchell and Soga 2005). Hence, a value of  $k_L = 2 \cdot 10^{-9}$  m/s was assumed for this study. The initial hydraulic conductivity of the sediments near the lake bottom was then calculated as

$$k_0 = k_L \cdot 10^{\frac{e_0 - e_L}{C_k}} \quad (9)$$

For the permeability change index, a value of  $C_k = C_c/1.5$  was assumed (Tavenas et al. 1983).

- Strength properties: The strength of the soil is defined by the inclination of the critical state line  $M$ . For the Zinnen slides, the value was chosen such that in the factor of safety of the slope in its in situ state is close to unity. For the more gentle Oberrieden Slope, assuming a factor of safety close to unity may not be reasonable, and the value  $M$  was chosen such that the predicted undrained shear resistance by the MCC constitutive model matches the measurements performed by Strupler et al. (2017) on undisturbed sediments adjacent to the slide (see also Appendix II).

The final values for the input parameters for the sedimentation analysis are summarized in Table 1.

## Appendix II. Derivation of the Input Soil Parameters for the Dynamic Analyses

Subsequently, the derivation of the input parameters for the dynamic analyses (seismic and postfailure) of the case studies is described. It should be pointed out that each parameter affects different aspects of the model behavior. Therefore, most model parameters cannot be determined independently. Instead, a set of parameters was determined that provides the best fit for the following aspects [a more detailed description of the model parameters is provided by Stoecklin et al. (2020)]:

- Initial shear stiffness: The initial shear modulus (see Fig. 9) was chosen as function of the vertical effective stress as  $G_0 = 200 \cdot \sigma'_v$  (Andersen 2015).
- Peak shear resistance: The undrained shear resistance was calibrated against in situ CPT measurements, which were taken in the undisturbed sediments adjacent to the Oberrieden (Strupler et al. 2017) and the Zinnen slides (Sammartini et al. 2021). The measured shear strength and the assumed static strength profile for the Oberrieden simulation are shown in Fig. 15. To account for the strain-rate dependency of the shear resistance, the undrained shear resistance was assumed about 25% higher for the dynamic seismic and postfailure analysis, compared with the static value (Lunne and Andersen 2007). For the Zinnen site, the undrained peak shear resistance was chosen such that the slope is marginally stable under static conditions prior to the collapse, rather than using the CPT measurements on the sediments. This approach was chosen, since the CPT measurements likely underestimate the undrained shear resistance in the steep part of the slope, where high static, drained shear stresses are acting. For more details, see Klein et al. (2022).
- Remolded shear resistance: The remoulded shear resistance was specified as a function of the initial peak shear resistance as  $s_{u,r} = s_{u,p}/S_t$ . For neither of the two sites, direct measurements of the remolded undrained shear resistance was available to the authors. Hence, for the Zinnen site, the parameter was estimated from measurements taken at the nearby Chrüttrichter site. For the latter, a sensitivity value of  $S_t \approx 2.0$  was measured on vane shear tests conducted on core samples of undisturbed sediments (Strasser et al. 2007). The same value was assumed for the analysis of the Zinnen slides, where similar lithological characteristics are present. For the Oberrieden site, Strupler et al. (2017) found that the gliding plane of the Oberrieden Slide 2 is located within the lithological unit LU1 (see Fig. 15), which consists of late glacial plastic mud. Measurements on late glacial mud at a site further up the shore in Richterswil revealed values for the sensitivity of  $S_t = 3 - 4$  (Gyger et al. 1976). For the analysis of the Oberrieden Slide 2, a value of  $S_t = 3$  was assumed. Assuming a value on the upper limit of the reported range, it should be mentioned, would likely result in less accurate prediction of the deformation front. In the simulations, the remolded shear resistance is defined through the parameter  $p'_{cs} = s_{u,r}/M_d$  (see Fig. 8). For the shear displacement, at which the remolded shear resistance is reached, a typical value of  $\delta_r = 0.2$  m was assumed (Skempton 1985).
- Stiffness degradation and damping: The nonlinear stress-strain behavior of the soil plays an important role for the dynamic response of the slope. To determine these values directly, cyclic laboratory tests on the sediments would be required. Since such tests are not available for the investigated sites, modulus



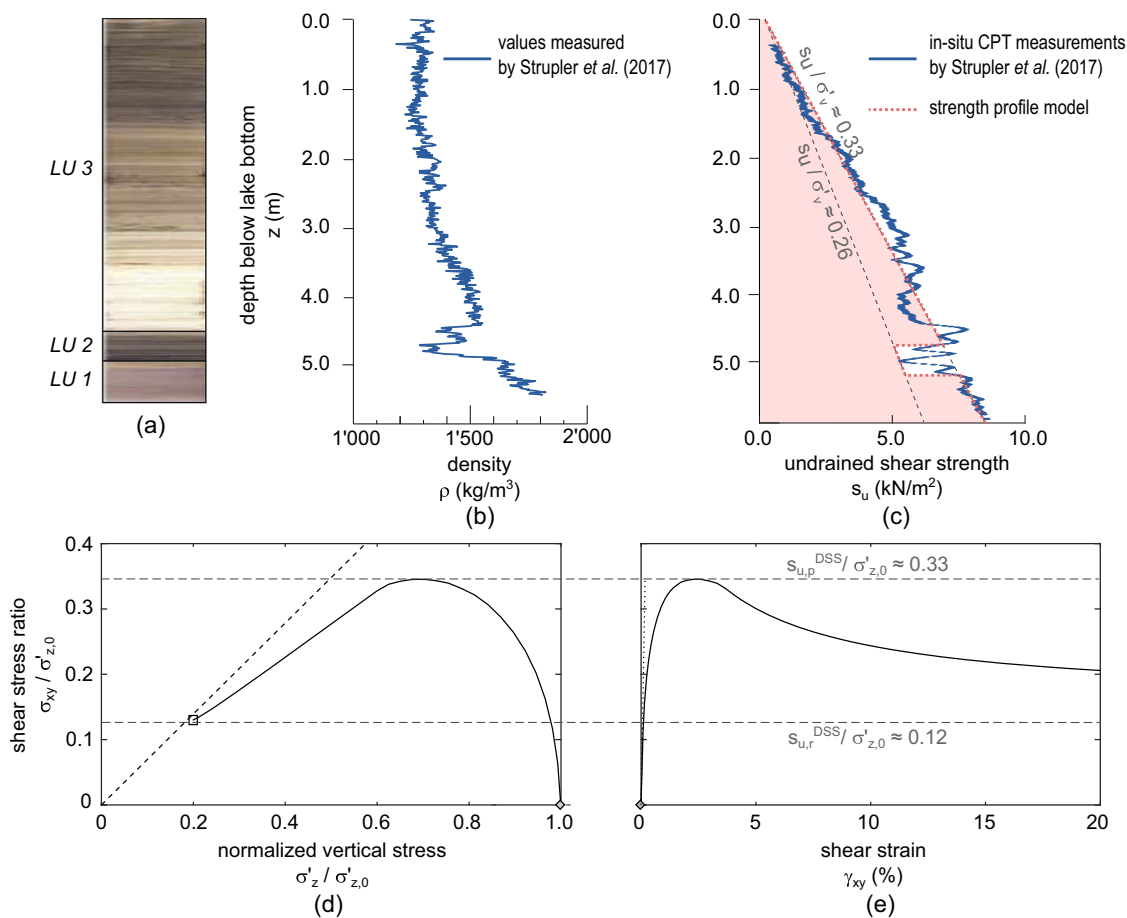


**Fig. 15.** Derivation of the shear strength properties for the Oberrieden Slide 2: (a) retrieved core; (b) measured density; and (c) measured undrained shear resistance by Strupler et al. (2017) compared with the strength profile assumed for the simulation. (d and e) Normalized response of the calibrated constitutive model. [Reprinted (a–c) with permission from Springer Link: Springer, *Geo-Marine Letters*, “Probabilistic stability evaluation and seismic triggering scenarios of submerged slopes in Lake Zurich (Switzerland),” M. Strupler, M. Hilbe, F. S. Anselmetti, A. J. Kopf, T. Fleischmann, and M. Strasser, © 2017.]

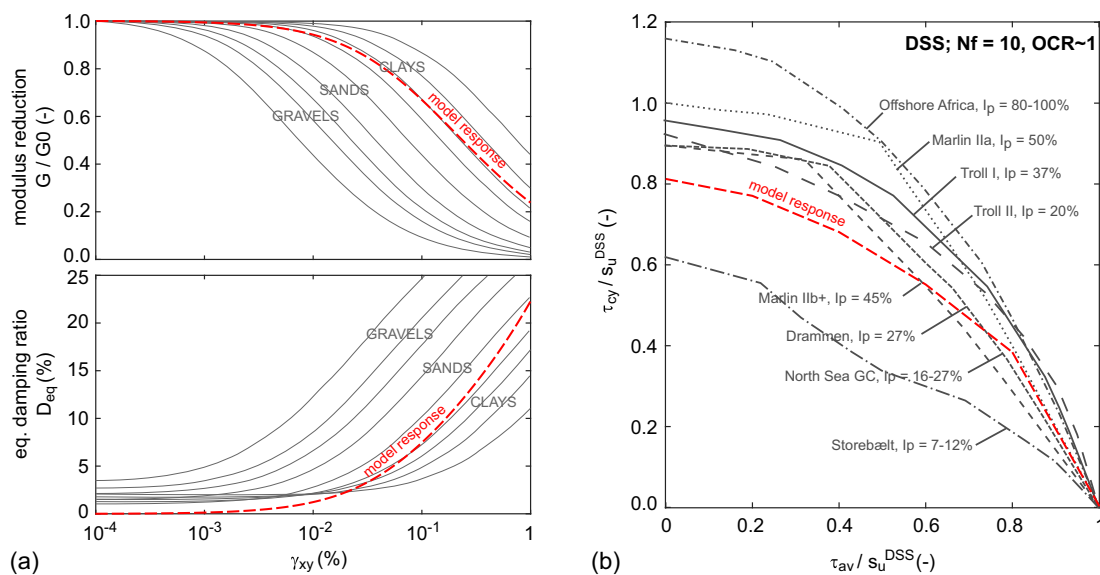


**Fig. 16.** Calibration of the stress–strain behaviour and cyclic degradation for the Oberrieden parameter set: (a) comparison of the calibrated model response with typical modulus reduction- and damping curves for different soil types (data from Darandeli 2001; EPRI 1993); and (b) results obtained from cyclic simple shear tests on various normally consolidated clays are compared with the calibrated model response for a simple shear element test. The diagram depicts combinations of sustained, average ( $\tau_{av}$ ), and cyclic shear stress ( $\tau_{cy}$ ) that caused failure of the samples after  $N_f = 10$  loading cycles (data from Andersen 2004).

**Table 2.** Summary of soil parameters for the seismic and postfailure analyses

Type	Parameter	Symbol	Value (Oberrieden slides)	Value (Zinnen slides)
Shear stiffness and damping	Hardening parameter 1	$h_0$	150	150
	Hardening parameter 2	$b$	2.1	2.1
Contraction and cyclic degradation	Initial contraction	$\beta_0$	-0.07	-0.07
	Dilation degradation parameter	$c$	2.0	2.0
	Shakedown parameter	$p'_1$	$0.6 \cdot p'_0$	$0.7 \cdot p'_0$
Strength parameters	Inclination failure surface soil layer	$M_{d,SL}$	1.3	2.2
	Weak layer	$M_{d,WL}$	0.95	1.8
	Normal effective stress at critical state	$p'_{cs}$	$0.2 \cdot p'_0$	$0.3 \cdot p'_0$

reduction and damping curves were used. The hardening parameters of the constitutive model, i.e., the parameters that define the shape of the deviatoric stress-strain curve  $h_0$  and  $b$  (Stoecklin et al. 2020) were calibrated such that the model response matches typical modulus reduction and damping curves (Darandeli 2001). This is illustrated in Fig. 16(a) for the Oberrieden parameter set.

- Cyclic degradation: The cyclic degradation of stiffness and strength is controlled by the pore-pressure buildup and plays an important role for the seismic response of the slope. In particular, predicting the number of stress cycles required to cause a failure is an important criteria. In absence of cyclic laboratory tests for the analyzed sites, typical values of number of cycles to failure are taken as a basis to calibrate this aspect of soil behavior. This was used to calibrate the initial contraction model parameter  $\beta_0$  and the shakedown parameter  $p'_1$ , which mainly define this aspect of the soil behavior (Stoecklin et al. 2020). This is depicted in Fig. 16(b), where the predicted response of the calibrated model for different loading combinations is compared with results from cyclic laboratory tests on various types of clays, published by Andersen (2004).

The derived set of parameters for the seismic and postfailure analyses is summarized in Table 2.

## Data Availability Statement

All data, models, and code generated or used during the study appear in the published article or are publically available from the referenced sources.

## Acknowledgments

The authors would like to thank Balz Friedli, Marc Kohler, Achim Kopf, and Mark Randolph for valuable discussions along the way to develop the framework. The work has been supported by the Swiss National Science Foundation, SNF Grant No. 200021\_168998.

## References

Alsardi, A., J. Copana, and A. Yerro. 2021. "Modelling earthquake-triggered landslide runout with the material point method." *Proc. Inst. Civ. Eng. Geotech. Eng.* 174 (5): 563–576. <https://doi.org/10.1680/jgeen.20.00235>.

Andersen, K. H. 2004. "Cyclic clay data for foundation design of structures subjected to wave loading." In *Cyclic behaviour of soils and liquefaction phenomena*, edited by Triantafyllidis, 371–387. London: Taylor & Francis.

Andersen, K. H. 2015. "Cyclic soil parameters for offshore foundation design." In *Frontiers in offshore geotechnics III*. London: CRC Press.

Audet, D. M., and A. C. Fowler. 1992. "A mathematical model for compaction in sedimentary basins." *Geophys. J. Int.* 110 (3): 577–590. <https://doi.org/10.1111/j.1365-246X.1992.tb02093.x>.

Benson, D. J. 1992. "Computational methods in Lagrangian and Eulerian hydrocodes." *Comput. Methods Appl. Mech. Eng.* 99 (2–3): 235–394. [https://doi.org/10.1016/0045-7825\(92\)90042-1](https://doi.org/10.1016/0045-7825(92)90042-1).

Bielak, J. 2003. "Domain reduction method for three-dimensional earthquake modeling in localized regions, Part I: Theory." *Bull. Seismol. Soc. Am.* 93 (2): 817–824. <https://doi.org/10.1785/0120010251>.

Biscontin, G., J. Pestana, and F. Nadim. 2004. "Seismic triggering of submarine slides in soft cohesive soil deposits." *Mar. Geol.* 203 (3–4): 341–354. [https://doi.org/10.1016/S0025-3227\(03\)00314-1](https://doi.org/10.1016/S0025-3227(03)00314-1).

Biscontin, G., and J. M. Pestana. 2006. "Factors affecting seismic response of submarine slopes." *Nat. Hazards Earth Syst. Sci.* 6 (1): 97–107. <https://doi.org/10.5194/nhess-6-97-2006>.

Buss, C., B. Friedli, and A. M. Puzrin. 2019. "Kinematic energy balance approach to submarine landslide evolution." *Can. Geotech. J.* 56 (9): 1351–1365. <https://doi.org/10.1139/cgj-2017-0651>.

Carter, L., J. D. Milliman, P. J. Talling, R. Gavey, and R. B. Wynn. 2012. "Near-synchronous and delayed initiation of long run-out submarine sediment flows from a record-breaking river flood, offshore Taiwan." *Geophys. Res. Lett.* 39 (12): 1–5. <https://doi.org/10.1029/2012GL051172>.

Darandeli, M. B. 2001. *Development of a new family of normalized modulus reduction and material damping curves*. Austin, TX: Univ. of Texas.

Dassault Systèmes. 2014. *Abaqus 6.14 documentation*. Providence, RI: Dassault Systèmes.

Dey, R., B. Hawlader, R. Phillips, and K. Soga. 2015. "Large deformation finite-element modelling of progressive failure leading to spread in sensitive clay slopes." *Géotechnique* 65 (8): 657–668. <https://doi.org/10.1680/geot.14.P193>.

Dey, R., B. Hawlader, R. Phillips, and K. Soga. 2016a. "Modeling of large-deformation behaviour of marine sensitive clays and its application to submarine slope stability analysis." *Can. Geotech. J.* 53 (7): 1138–1155. <https://doi.org/10.1139/cgj-2015-0176>.

Dey, R., B. C. Hawlader, R. Phillips, and K. Soga. 2016b. "Numerical modelling of submarine landslides with sensitive clay layers." *Géotechnique* 66 (6): 454–468. <https://doi.org/10.1680/jgeot.15.P111>.

Dugan, B., and T. C. Sheahan. 2012. "Offshore sediment overpressures of passive margins: Mechanisms, measurement, and models." *Rev. Geophys.* 50 (3): 271–276. <https://doi.org/10.1029/2011RG000379>.

EPRI (Electric Power Research Institute). 1993. *Guidelines for determining design basis ground motions*. Palo Alto, CA: EPRI.

Fine, I. V., A. B. Rabinovich, B. D. Bornhold, R. E. Thomson, and E. A. Kulikov. 2005. "The Grand Banks landslide-generated tsunamis of November 18, 1929: Preliminary analysis and numerical modeling." *Mar. Geol.* 215 (1–2): 45–57. <https://doi.org/10.1016/j.margeo.2004.11.007>.

Fisher, M. A., W. R. Normark, H. G. Greene, H. J. Lee, and R. W. Sliter. 2005. "Geology and tsunamigenic potential of submarine landslides

- in Santa Barbara Channel, Southern California." *Mar. Geol.* 224 (1–4): 1–22. <https://doi.org/10.1016/j.margeo.2005.07.012>.
- Fryer, G. J., P. Watts, and L. F. Pratson. 2004. "Source of the great tsunami of 1 April 1946: A landslide in the upper Aleutian forearc." *Mar. Geol.* 203 (3–4): 201–218. [https://doi.org/10.1016/S0025-3227\(03\)00305-0](https://doi.org/10.1016/S0025-3227(03)00305-0).
- Germanovich, L. N., S. Kim, and A. M. Puzrin. 2016. "Dynamic growth of slip surfaces in catastrophic landslides." *Proc. R. Soc. A: Math. Phys. Eng. Sci.* 472 (2185): 20150758. <https://doi.org/10.1098/rspa.2015.0758>.
- Gibson, R. E. 1958. "The progress of consolidation in a clay layer increasing in thickness with time." *Géotechnique* 8 (4): 171–182. <https://doi.org/10.1680/geot.1958.8.4.171>.
- Gyger, M., M. Müller-Vonmoos, and C. Schindler. 1976. "Untersuchungen zur Klassifikation spät- und nacheiszeitlicher Sedimente aus dem Zürichsee." *Schweiz. Mineral. Petrogr. Mitt.* 2 (56): 387–406.
- Hampton, M. A., H. J. Lee, and J. Locat. 1996. "Submarine landslides." *Rev. Geophys.* 34 (1): 33–59. <https://doi.org/10.1029/95RG03287>.
- Klein, B., A. M. Puzrin, A. Stoecklin, and A. Kopf. 2022. "Basin sediments geometry and strength as controls for post-failure emplacement style of alpine sub-lacustrine landslides." *J. Geophys. Res. Solid Earth* 127 (10): e2022JB024614. <https://doi.org/10.1029/2022JB024614>.
- Kohler, M., A. Stoecklin, and A. M. Puzrin. 2022. "A MPM framework for large-deformation seismic response analysis." *Can. Geotech. J.* 59 (6): 1046–1060. <https://doi.org/10.1139/cgj-2021-0252>.
- Kremer, K., S. B. Wirth, A. Reusch, D. Fäh, B. Bellwald, F. S. Anselmetti, S. Girardclos, and M. Strasser. 2017. "Lake-sediment based paleoseismology: Limitations and perspectives from the Swiss Alps." *Quat. Sci. Rev.* 168 (Jul): 1–18. <https://doi.org/10.1016/j.quascirev.2017.04.026>.
- Kvalstad, T. J., L. Andresen, C. F. Forsberg, K. Berg, P. Bryn, and M. Wangen. 2005. "The Storegga slide: Evaluation of triggering sources and slide mechanics." *Mar. Pet. Geol.* 22 (1–2): 245–256. <https://doi.org/10.1016/j.marpetgeo.2004.10.019>.
- Ladd, C. C., and L. Edgers. 1972. *Consolidated-undrained direct-simple shear tests on saturated clays*. Cambridge, MA: Massachusetts Institute of Technology.
- Laue, J. 2014. "Allgemeine Konzepte des seismischen Entwurfs und der Bemessung in der Geotechnik mit Anwendung auf Hänge." *Mitteilungen der Geotechnik Schweiz* 168: 37–52.
- Lee, H. J., J. Locat, P. Desgagns, J. D. Parsons, B. G. McAdoo, D. L. Orange, P. Puig, F. L. Wong, P. Dartnell, and E. Boulanger. 2007. "Submarine mass movements on continental margins." In *Continental margin sedimentation*, 213–274. Oxford, UK: Blackwell Publishing.
- Locat, J., and H. J. Lee. 2002. "Submarine landslides: Advances and challenges." *Can. Geotech. J.* 39 (1): 193–212. <https://doi.org/10.1139/t01-089>.
- Løvholt, F., S. Bondevik, J. S. Laberg, J. Kim, and N. Boylan. 2017. "Some giant submarine landslides do not produce large tsunamis." *Geophys. Res. Lett.* 44 (16): 8463–8472. <https://doi.org/10.1002/2017GL074062>.
- Lunne, T., and K. H. Andersen. 2007. "Soft clay shear strength parameters for deepwater geotechnical design." In *Proc., 6th Int. Conf. on Offshore Site Investigation and Geotechnics: Confronting New Challenges and Sharing Knowledge*. Richardson, TX: OnePetro.
- Masson, D., A. Watts, M. J. Gee, R. Urgeles, N. Mitchell, T. Le Bas, and M. Canals. 2002. "Slope failures on the flanks of the western Canary Islands." *Earth Sci. Rev.* 57 (1–2): 1–35. [https://doi.org/10.1016/S0012-8252\(01\)00069-1](https://doi.org/10.1016/S0012-8252(01)00069-1).
- Masson, D. G., C. B. Harbitz, R. B. Wynn, G. Pedersen, and F. Løvholt. 2006. "Submarine landslides: Processes, triggers and hazard prediction." *Philos. Trans. R. Soc. A Math. Phys. Eng. Sci.* 364 (1845): 2009–2039. <https://doi.org/10.1098/rsta.2006.1810>.
- Mejia, L. H., and E. M. Dawson. 2006. "Earthquake deconvolution for FLAC." In *Proc., 4th Int. FLAC Symp. on Numerical Modeling in Geomechanics*, Hart and Varona, 211–219. Minneapolis: Itasca Consulting Group.
- Mesri, G., and A. Rokhsar. 1974. "Theory of consolidation of clays." *ASCE J. Geotech. Eng. Div.* 100 (8): 889–904. <https://doi.org/10.1061/AJGEB6.0000075>.
- Mitchell, J. K., and K. Soga. 2005. *Fundamentals of soil behavior*. Hoboken, NJ: Wiley.
- Mohrig, D., C. Ellis, G. Parker, K. X. Whipple, and M. Hondzo. 1998. "Hydroplaning of subaqueous debris flows." *Geol. Soc. Am. Bull.* 110 (3): 387–394. [https://doi.org/10.1130/0016-7606\(1998\)110<0387:HOSDF>2.3.CO;2](https://doi.org/10.1130/0016-7606(1998)110<0387:HOSDF>2.3.CO;2).
- Montáns, F. J. 2001. "Implicit multilayer J2-plasticity using Prager's translation rule." *Int. J. Numer. Methods Eng.* 50 (2): 347–375. [https://doi.org/10.1002/1097-0207\(20010120\)50:2%3C347::AID-NME28%3E3.0.CO;2-Q](https://doi.org/10.1002/1097-0207(20010120)50:2%3C347::AID-NME28%3E3.0.CO;2-Q).
- Mosher, D. C., L. Moscardelli, R. C. Shipp, J. D. Chaytor, C. D. P. Baxter, H. J. Lee, and R. Urgeles. 2010. *Submarine mass movements and their consequences*, 1–8. Dordrecht, Netherlands: Springer.
- Nadim, F., G. Biscontin, and A. M. Kaynia. 2007. "Seismic triggering of submarine slides." In *Proc., Offshore Technology Conf.*, 1–8. Richardson, TX: OnePetro. <https://doi.org/10.4043/18911-MS>.
- Nielsen, A. H. 2014. "Towards a complete framework for seismic analysis in Abaqus." *Proc. Inst. Civ. Eng.: Eng. Comput. Mech.* 167 (1): 3–12. <https://doi.org/10.1680/eacm.12.00004>.
- Palmer, A. C., and J. R. Rice. 1973. "The growth of slip surfaces in the progressive failure of over-consolidated clay." *Proc. R. Soc. A: Math. Phys. Eng. Sci.* 332 (1591): 527–548. <https://doi.org/10.1098/rspa.1973.0040>.
- Prevost, J. H. 1985. "A simple plasticity theory for frictional cohesionless soils." *Int. J. Soil Dyn. Earthquake Eng.* 4 (1): 9–17. [https://doi.org/10.1016/0261-7277\(85\)90030-0](https://doi.org/10.1016/0261-7277(85)90030-0).
- Puzrin, A., S. Frydman, and M. Talesnick. 1997. "Effect of degradation on seismic response of Israeli continental slope." *J. Geotech. Geoenviron. Eng.* 123 (2): 85–93. [https://doi.org/10.1061/\(ASCE\)1090-0241\(1997\)123:2\(85\)](https://doi.org/10.1061/(ASCE)1090-0241(1997)123:2(85)).
- Puzrin, A. M., L. N. Germanovich, and B. Friedli. 2016. "Shear band propagation analysis of submarine slope stability." *Géotechnique* 66 (3): 188–201. <https://doi.org/10.1680/jgeot.15.LM.002>.
- Puzrin, A. M., L. N. Germanovich, and S. Kim. 2004. "Catastrophic failure of submerged slopes in normally consolidated sediments." *Géotechnique* 54 (10): 631–643. <https://doi.org/10.1680/geot.2004.54.10.631>.
- Puzrin, A. M., T. E. Gray, and A. J. Hill. 2015. "Significance of the actual nonlinear slope geometry for catastrophic failure in submarine landslides." *Proc. R. Soc. A: Math. Phys. Eng. Sci.* 471 (2175): 20140772. <https://doi.org/10.1098/rspa.2014.0772>.
- Randolph, M. F., and S. Gourvenec. 2011. *Offshore geotechnical engineering*. Hoboken, NJ: Taylor & Francis.
- Roscoe, K. H., and J. B. Burland. 1970. "On the generalized stress-strain behavior of 'wet' clay." *J. Terramech.* 7 (2): 107–108.
- Sammartini, M., J. Moernaut, A. Kopf, S. Stegmann, S. C. Fabbri, F. S. Anselmetti, and M. Strasser. 2021. "Propagation of frontally confined subaqueous landslides: Insights from combining geophysical, sedimentological, and geotechnical analysis." *Sediment. Geol.* 416 (Apr): 105877. <https://doi.org/10.1016/j.sedgeo.2021.105877>.
- Sawyer, D. E., and J. R. Devore. 2015. "Elevated shear strength of sediments on active margins: Evidence for seismic strengthening." *Geophys. Res. Lett.* 42 (23): 10216–10221. <https://doi.org/10.1002/2015GL066603>.
- Sawyer, D. E., R. S. Reece, S. P. S. Gulick, and B. L. Lenz. 2017. "Submarine landslide and tsunami hazards offshore southern Alaska: Seismic strengthening versus rapid sedimentation." *Geophys. Res. Lett.* 44 (16): 8435–8442. <https://doi.org/10.1002/2017GL074537>.
- Schnellmann, M., F. S. Anselmetti, D. Giardini, and J. A. Mckenzie. 2006. "15,000 Years of mass-movement history in Lake Lucerne: Implications for seismic and tsunami hazards." *Eclogae Geol. Helv.* 99 (3): 409–428. <https://doi.org/10.1007/s00015-006-1196-7>.
- Schnellmann, M., F. S. Anselmetti, D. Giardini, and J. A. McKenzie. 2005. "Mass movement-induced fold-and-thrust belt structures in unconsolidated sediments in Lake Lucerne (Switzerland)." *Sedimentology* 52 (2): 271–289. <https://doi.org/10.1111/j.1365-3091.2004.00694.x>.
- Schnellmann, M., F. S. Anselmetti, D. Giardini, J. A. McKenzie, and S. N. Ward. 2002. "Prehistoric earthquake history revealed by lacustrine slump deposits." *Geology* 30 (12): 1131–1134. [https://doi.org/10.1130/0091-7613\(2002\)030<1131:PEHRBL>2.0.CO;2](https://doi.org/10.1130/0091-7613(2002)030<1131:PEHRBL>2.0.CO;2).
- Skempton, A. W. 1985. "Residual strength of clays in landslides, folded strata and the laboratory." *Géotechnique* 35 (1): 3–18. <https://doi.org/10.1680/geot.1985.35.1.3>.



- Soga, K., E. Alonso, A. Yerro, K. Kumar, and S. Bandara. 2016. "Trends in large-deformation analysis of landslide mass movements with particular emphasis on the material point method." *Géotechnique* 66 (3): 248–273. <https://doi.org/10.1680/jgeot.15.LM.005>.
- Stigall, J., and B. Dugan. 2010. "Overpressure and earthquake initiated slope failure in the Ursa region, northern Gulf of Mexico." *J. Geophys. Res.* 115 (B4): B04101. <https://doi.org/10.1029/2009JB006848>.
- Stoecklin, A., B. Friedli, and A. M. Puzrin. 2017. "Sedimentation as a control for large submarine landslides: Mechanical modeling and analysis of the Santa Barbara Basin." *J. Geophys. Res. Solid Earth* 122 (11): 8645–8663. <https://doi.org/10.1002/2017JB014752>.
- Stoecklin, A., B. Friedli, and A. M. Puzrin. 2020. "A multisurface kinematic hardening model for the behavior of clays under combined static and undrained cyclic loading." *Int. J. Numer. Anal. Methods Geomech.* 44 (17): 2358–2387. <https://doi.org/10.1002/nag.3149>.
- Stoecklin, A., and A. M. Puzrin. 2020. "A combined analysis procedure for submarine landslide evolution." In *Proc., 4th Int. Symp. on Frontiers in Offshore Geotechnics*, 878–886. Hawthorne, NJ: Deep Foundation Institute.
- Stoecklin, A., P. Trapper, and A. M. Puzrin. 2021. "Controlling factors for post-failure evolution of subaqueous landslides." *Géotechnique* 71 (10): 879–892. <https://doi.org/10.1680/jgeot.19.P.230>.
- Strasser, M., and F. S. Anselmetti. 2008. "Mass-movement event stratigraphy in Lake Zurich: A record of varying seismic and environmental impacts." *Beiträge zur Geologie der Schweiz, Geotechnische Serie* 95: 23–41.
- Strasser, M., P. Henry, T. Kanamatsu, M. K. Thu, and G. F. Moore. 2012. "Scientific drilling of mass transport deposits in the Nankai accretionary wedge: First results from IODP expedition 333." In *Proc., Submarine Mass Movements and Their Consequences—5th Int. Symp.*, 671–681. Dordrecht, Netherlands: Springer. [https://doi.org/10.1007/978-94-007-2162-3\\_60](https://doi.org/10.1007/978-94-007-2162-3_60).
- Strasser, M., M. Hilbe, and F. S. Anselmetti. 2011. "Mapping basin-wide subaqueous slope failure susceptibility as a tool to assess regional seismic and tsunami hazards." *Mar. Geophys. Res.* 32 (1–2): 331–347. <https://doi.org/10.1007/s11001-010-9100-2>.
- Strasser, M., K. Monecke, M. Schnellmann, and F. S. Anselmetti. 2013. "Lake sediments as natural seismographs: A compiled record of Late Quaternary earthquakes in Central Switzerland and its implication for Alpine deformation." *Sedimentology* 60 (1): 319–341. <https://doi.org/10.1111/sed.12003>.
- Strasser, M., S. Stegmann, F. Bussmann, F. S. Anselmetti, B. Rick, and A. Kopf. 2007. "Quantifying subaqueous slope stability during seismic shaking: Lake Lucerne as model for ocean margins." *Mar. Geol.* 240 (1–4): 77–97. <https://doi.org/10.1016/j.margeo.2007.02.016>.
- Strozyk, F., M. Strasser, A. Frster, A. Kopf, and K. Huhn. 2010. "Slope failure repetition in active margin environments: Constraints from submarine landslides in the Hellenic fore arc, eastern Mediterranean." *J. Geophys. Res. Solid Earth* 115 (B8). <https://doi.org/10.1029/2009JB006841>.
- Strupler, M., M. Hilbe, F. S. Anselmetti, A. J. Kopf, T. Fleischmann, and M. Strasser. 2017. "Probabilistic stability evaluation and seismic triggering scenarios of submerged slopes in Lake Zurich (Switzerland)." *Geo-Mar. Lett.* 37 (3): 241–258. <https://doi.org/10.1007/s00367-017-0492-8>.
- Tappin, D. R., P. Watts, G. M. McMurtry, Y. Lafoy, and T. Matsumoto. 2001. "The Sissano, Papua New Guinea tsunami of July 1998—Offshore evidence on the source mechanism." *Mar. Geol.* 175 (1–4): 1–23. [https://doi.org/10.1016/S0025-3227\(01\)00131-1](https://doi.org/10.1016/S0025-3227(01)00131-1).
- Tavenas, F., P. Jean, P. Leblond, S. Leroueil, and E. Juárez-Badillo. 1983. "The permeability of natural soft clays. Part II: Permeability characteristics." *Can. Geotech. J.* 20 (4): 645–660. <https://doi.org/10.1139/t83-073>.
- ten Brink, U. S., B. D. Andrews, and N. C. Miller. 2016. "Seismicity and sedimentation rate effects on submarine slope stability." *Geology* 44 (7): 563–566. <https://doi.org/10.1130/G37866.1>.
- Trapper, P. A., A. M. Puzrin, and L. N. Germanovich. 2015. "Effects of shear band propagation on early waves generated by initial breakoff of tsunamigenic landslides." *Mar. Geol.* 370 (Dec): 99–112. <https://doi.org/10.1016/j.margeo.2015.10.014>.
- Vanneste, M., N. Sultan, S. Garziglia, C. F. Forsberg, and J.-S. L'Heureux. 2014. "Seafloor instabilities and sediment deformation processes: The need for integrated, multi-disciplinary investigations." *Mar. Geol.* 352 (Jun): 183–214. <https://doi.org/10.1016/j.margeo.2014.01.005>.
- Viesca, R. C., and J. R. Rice. 2012. "Nucleation of slip-weakening rupture instability in landslides by localized increase of pore pressure." *J. Geophys. Res. Solid Earth* 117 (B3). <https://doi.org/10.1029/2011JB008866>.
- Völker, D., F. Scholz, and J. Geersen. 2011. "Analysis of submarine landslide in the rupture area of the 27 February 2010 Maule earthquake, Central Chile." *Mar. Geol.* 288 (1–4): 79–89. <https://doi.org/10.1016/j.margeo.2011.08.003>.
- Wangen, M. 1992. "Pressure and temperature evolution in sedimentary basins." *Geophys. J. Int.* 110 (3): 601–613. <https://doi.org/10.1111/j.1365-246X.1992.tb02095.x>.
- Zhang, W., M. F. Randolph, A. M. Puzrin, and D. Wang. 2019. "Transition from shear band propagation to global slab failure in submarine landslides." *Can. Geotech. J.* 56 (4): 554–569. <https://doi.org/10.1139/cgj-2017-0648>.
- Zhang, W., D. Wang, M. F. Randolph, and A. M. Puzrin. 2015. "Catastrophic failure in planar landslides with a fully softened weak zone." *Géotechnique* 65 (9): 755–769. <https://doi.org/10.1680/geot14.P.218>.
- Zhang, W., D. Wang, M. F. Randolph, and A. M. Puzrin. 2017. "From progressive to catastrophic failure in submarine landslides with curvilinear slope geometries." *Géotechnique* 67 (12): 1104–1119. <https://doi.org/10.1680/jgeot.16.P.249>.
- Zhou, Y.-G., J. Chen, Y. She, A. M. Kaynia, B. Huang, and Y.-M. Chen. 2017. "Earthquake response and sliding displacement of submarine sensitive clay slopes." *Eng. Geol.* 227 (Sep): 69–83. <https://doi.org/10.1016/j.enggeo.2017.05.004>.
- Zienkiewicz, O. C., N. Bicanic, and F. Q. Shen. 1989. "Earthquake input definition and the transmitting boundary conditions." In *Advances in computational nonlinear mechanics*, 109–138. Berlin: Springer.